Published in final edited form as:

Cell Metab. 2022 February 01; 34(2): 317–328.e6. doi:10.1016/j.cmet.2021.12.024.

FGF21 suppresses alcohol consumption through an amygdalo-striatal circuit

Kyle H. Flippo[1,2,3,*,#], **Samuel A.J. Trammell**[5,†,*], **Matthew P. Gillum**[5,*], **Iltan Aklan**[1,2,3], **Misty B. Perez**[1,2,3], **Yavuz Yavuz**[1,2,3,††], **Nicholas K. Smith**[6], **Sharon O. Jensen-Cody**[1,2,3], **Bolu Zhou**[1,2,3], **Kristin E. Claflin**[1,2,3], **Amy Beierschmitt**[7,8], **Anders Fink-Jensen**[9], **Filip K. Knop**[10,11], **Roberta M. Palmour**[8,12], **Brad A. Grueter**[6], **Deniz Atasoy**[1,2,3], **Matthew J. Potthoff**[1,2,3,4,#,β]

[1]Department of Neuroscience and Pharmacology, University of Iowa Carver College of Medicine, Iowa City, IA 52242, USA

[2]Fraternal Order of Eagles Diabetes Research Center, University of Iowa Carver College of Medicine, Iowa City, IA 52242, USA

[3]Iowa Neuroscience Institute, University of Iowa Carver College of Medicine, Iowa City, IA 52242, USA

[4]Department of Veterans Affairs Medical Center, Iowa City, IA 52242, USA

[5]Section for Nutrient and Metabolite Sensing, the Novo Nordisk Foundation Center for Basic Metabolic Research, University of Copenhagen, 2200 Copenhagen, Denmark

[6]Department of Anesthesiology, Vanderbilt University, Nashville, TN 37323, USA.

[7]School of Veterinary Medicine, Ross University, Basseterre KN 0101, Saint Kitts and Nevis

[8]Behavioral Science Foundation, Basseterre KN 0101, Saint Kitts and Nevis

[#]Corresponding Authors: Matthew J. Potthoff, University of Iowa, 169 Newton Road, 3322 PBDB, Iowa City, IA 52242, Phone: 319-384-4438, matthew-potthoff@uiowa.edu, Kyle H. Flippo, University of Iowa, 169 Newton Road, 3322 PBDB, Iowa City, IA 52242, Phone: 319-384-4438, kyle-flippo@uiowa.edu.

[*]= These authors contributed equally

β= Lead contact

†= Current affiliation: Department of Biomedical Sciences, University of Copenhagen, 2200 Copenhagen, Denmark

††= Current affiliation: Department of Physiology, Yeditepe University Medical School, 34755 Istanbul, Turkey

Author contributions

M.J.P. and K.H.F. conceived of the project, designed experiments, interpreted data, wrote the paper, and are responsible for the integrity of its content. S.A.J.T. and M.P.G. conceived of the project, designed and performed experiments and interpreted data. I.A., Y.Y., S.O.J., M.B.P., B.Z., K.E.C., A.B., A.F.J., N.K.S., F.K.K., R.M.P., B.A.G., and D.A. performed experiments and interpreted data.

Declaration of interests

Recombinant human FGF21 protein was provided by Novo Nordisk and PF-05231023 was provided by Pfizer. Neither Novo Nordisk nor Pfizer was involved with the conceptualization, design, data collection, analysis, or preparation of the manuscript. Correspondence and requests for materials should be addressed to M.J.P.

Inclusion and diversity statement

One or more of the authors of this paper self-identifies as an underrepresented ethnic minority in science, and one or more of the authors of this paper received support from a program designed to increase minority representation in science.

[9]Laboratory of Neuropsychiatry, Psychiatric Centre Copenhagen and University Hospital of Copenhagen, Edel Sauntes Allé 10, DK-2100, Copenhagen, Denmark

[10]Center for Clinical Metabolic Research, Gentofte Hospital, University of Copenhagen, Gentofte Hospitalsvej 7, 3rd floor, DK- 2900, Hellerup, Denmark

[11]Steno Diabetes Center Copenhagen, 2820 Gentofte, Denmark

[12]Departments of Psychiatry and Human Genetics, McGill University, Montreal, QC, Canada

Summary

Excessive alcohol consumption is a major health and social issue in our society. Pharmacologic administration of the endocrine hormone fibroblast growth factor 21 (FGF21) suppresses alcohol consumption through actions in the brain in rodents, and genome wide association studies have identified single nucleotide polymorphisms in genes involved with FGF21 signaling as being associated with increased alcohol consumption in humans. However, the neural circuit(s) through which FGF21 signals to suppress alcohol consumption are unknown, as are its effects on alcohol consumption in higher organisms. Here, we demonstrate that administration of an FGF21 analogue to alcohol-preferring non-human primates reduces alcohol intake by 50%. Further, we reveal that FGF21 suppresses alcohol consumption through a projection-specific sub-population of KLB-expressing neurons in the basolateral amygdala. Our results illustrate how FGF21 suppresses alcohol consumption through a specific population of neurons in the brain and demonstrate its therapeutic potential in non-human primate models of excessive alcohol consumption.

eTOC blurb

Flippo, Trammell, Gillum et al. report that the FGF21 analogue PF-05231023 suppresses alcohol consumption in alcohol-preferring non-human primates. FGF21 signals to KLB-expressing neurons in the basolateral amygdala which project to the nucleus accumbens to suppress alcohol consumption. The circuit through which FGF21 suppresses alcohol consumption is distinct from that which it suppresses sucrose consumption.

Graphical Abstract

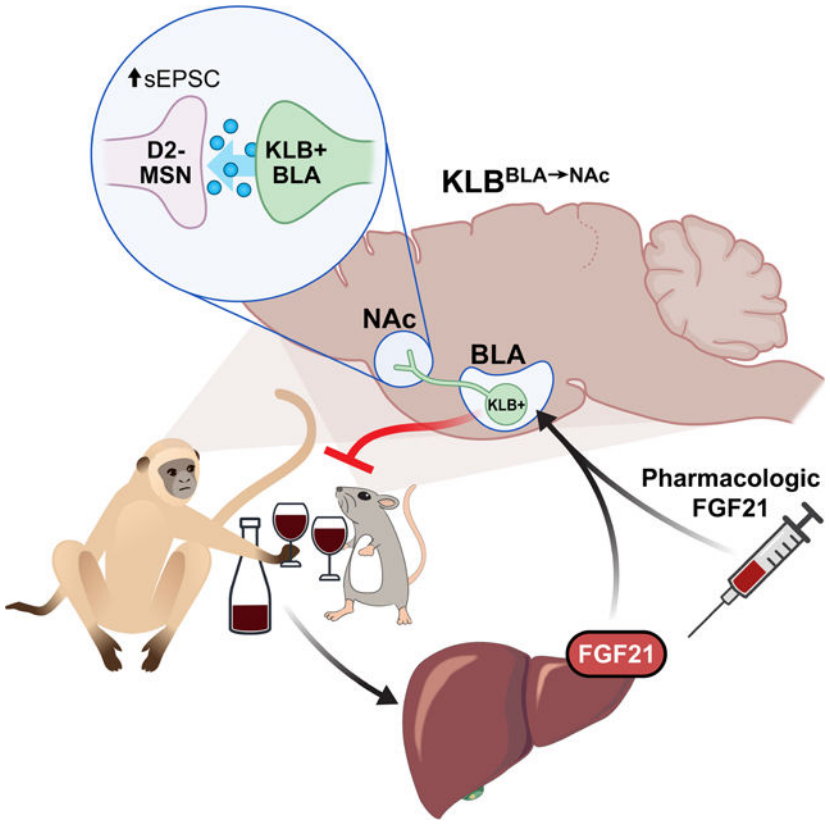

Keywords

FGF21; alcohol consumption; basolateral amygdala; nucleus accumbens; brain; liver; hepatokine

Introduction

Mammals began consuming alcohol from fermented fruit long before humans developed methods to produce alcohol from distillation. Given that excessive alcohol consumption negatively impacts health and survival, it is not surprising that numerous physiological systems have evolved to sense and regulate alcohol consumption in mammals. However, these homeostatic systems are subject to dysregulation due to genetic or environmental factors, which is evident in the high prevalence of alcohol dependence (Edenberg and Foroud, 2013). Efforts to therapeutically target pathways which contribute to regulation of alcohol consumption (i.e., ethanol metabolism (Haass-Koffler et al., 2017), reward signaling (Koob et al., 1998), or neuropeptide signaling (Thiele, 2017)) with the goal of cessation of alcohol consumption, have been limited in their efficacy to effectively treat alcohol use disorder (AUD) (Pomrenze et al., 2017; Swift and Aston, 2015; Trudell et al., 2014).

Recently, genome wide association studies identified multiple SNPs in the genes *FGF21* (Soberg et al., 2017) and *KLB* (Clarke et al., 2017; Jorgenson et al., 2017; Kranzler et al., 2019; Mallard et al., 2021; Sanchez-Roige et al., 2019; Schumann et al., 2016) as being associated with increased alcohol consumption in humans. KLB encodes the protein

β-klotho which is an obligate co-receptor for biological activities of the endocrine hormone fibroblast growth factor 21 (FGF21) (Adams et al., 2012; Ding et al., 2012; Kurosu et al., 2007; Wu et al., 2007). FGF21 is produced from the liver in response to metabolic and nutritional challenges and functions to regulate energy homeostasis and macronutrient balance (BonDurant and Potthoff, 2018; Flippo and Potthoff, 2021). FGF21 crosses the blood brain barrier (Hsuchou et al., 2007) and FGF21 signaling to the CNS is important for its effects to modulate energy balance and macronutrient preference (Ameka et al., 2019; Jensen-Cody et al., 2020; Owen et al., 2014; von Holstein-Rathlou et al., 2016). Recently, FGF21 signaling has also been shown to regulate alcohol consumption. Both FGF21 transgenic expression (Talukdar et al., 2016a) and pharmacologic administration of FGF21 (Schumann *et al.*, 2016) reduce alcohol preference in mice through direct FGF21 signaling to the central nervous system. While previous work has described an association between dopamine levels in the brain and FGF21 administration (Talukdar *et al.*, 2016a), the precise neural circuits through which FGF21 mediates suppression of alcohol consumption are unknown. Moreover, whether FGF21 is capable of inhibiting alcohol consumption in higher order mammals has not been investigated. Here, we demonstrate the potential translational impact of FGF21-based therapeutics in suppressing alcohol consumption in alcohol-preferring non-human primates, vervet monkeys (*Chlorocebus sabaeus*) and reveal that FGF21 alters glutamatergic transmission in the nucleus accumbens and suppresses alcohol consumption through a projection-specific sub- population of KLB-expressing neurons in the basolateral amygdala.

Results

Endogenous FGF21 and pharmacologic administration of FGF21 suppress alcohol consumption in rodents and non-human primates.

Both chronic alcohol consumption and acute binge-like consumption increase circulating levels of endogenous FGF21 (Desai et al., 2017; Liu et al., 2016; Soberg et al., 2018; Wagner-Skacel et al., 2021). To determine if circulating FGF21 induced by ethanol consumption is derived from the liver, as is the case for many nutritional challenges (Flippo and Potthoff, 2021), we deleted FGF21 in the liver by administering AAV viruses expressing either Cre-recombinase or a control construct under a liver-specific promoter (AAV-TBG-Cre and AAV-TBG-Con, respectively) to mice harboring a floxed FGF21 allele ($FGF21^{fl/fl}$) (Fig. S1A,B). Consistent with previous studies, ethanol consumption significantly increased circulating levels of FGF21 following ethanol gavage in AAV-TBG-Con expressing $FGF21^{fl/fl}$ mice relative to littermates receiving a water gavage (Fig. 1A). In contrast, deletion of FGF21 from the liver by administration of AAV-TBG-Cre to $FGF21^{fl/fl}$ mice (Fig. S1A and S1B) completely abolished the induction of circulating levels of FGF21 following ethanol gavage (Fig. 1A), demonstrating that circulating levels of FGF21 induced by ethanol originate primarily from the liver. To determine whether liver-derived FGF21 functions in a homeostatic fashion to regulate alcohol consumption, we measured *ad libitum* alcohol consumption in both $FGF21^{fl/fl}$ mice expressing either AAV-TBG-Cre or AAV-TBG-Con (Fig. 1B), and in mice in which FGF21 was constitutively deleted from the liver by crossing $FGF21^{fl/fl}$ mice with Albumin-Cre transgenic mice (FGF21 LivKO; (Markan et al., 2014)) (Fig. 1C). In both cases, deletion of FGF21 from the liver significantly increased

ethanol consumption compared to wild-type (WT) littermate controls (Fig. 1B,C). These data suggest that liver-derived FGF21 functions in a homeostatic fashion to decrease alcohol consumption. Consistent with these data, intraperitoneal (IP) administration of recombinant human FGF21 to WT mice significantly decreased alcohol consumption in a dose-dependent manner in a two-bottle choice experiment with alcohol versus water (Fig. 1D), in agreement with previous work (Schumann *et al.*, 2016). In addition, FGF21 administration also decreased alcohol intake when mixed in with a liquid diet (Lieber-DeCarli) (Fig. 1E). Recombinant FGF21 administration did not influence EtOH metabolism (Fig. 1F) or rotarod performance following EtOH gavage (Fig. S1C).

To extend these findings to potential therapeutic applications, we administered a long-acting FGF21 analogue, PF-05231023 (Talukdar et al., 2016b), to mice and measured alcohol consumption by two-bottle choice. PF-05231023 administration significantly reduced ethanol consumption compared to vehicle treated mice (Fig. 1G). We next assessed the effect of PF-05231023 on an intermittent access model of ethanol consumption which is an assay that drives higher levels of ethanol consumption (Hwa et al., 2011). As expected, intermittent access of alcohol significantly increased ethanol consumption in vehicle treated mice compared to the intake observed with the two-bottle choice assay. Notably, PF-05231023 administration significantly reduced (~50%) ethanol consumption in both male (Fig. 1H) and female (Fig. 1I) mice compared to vehicle treated controls. PF-05231023 did not alter patterns of ethanol consumption, but instead decreased the amount of alcohol consumed during periods of consumption (Fig. S1D-F).

To determine whether PF-05231023 also reduces alcohol consumption in higher-order mammals, we performed similar experiments in alcohol-preferring non-human primates, vervet monkeys (*Chlorocebus sabaeus*). The vervet monkey population comprises alcohol avoiders, moderate alcohol drinkers, and a group of heavy drinkers (Ervin et al., 1990; Palmour et al., 1997). The heavy drinkers will consume alcohol to intoxication if possible, thereby offering a preclinical model of alcohol drinking that may more closely reflect aspects of harmful drinking in humans. Importantly, PF-05231023 also reduced ethanol consumption in alcohol preferring vervet non- human primates compared to vehicle treated controls (Fig. 1J,K) without significantly altering water intake (Fig. 1L) or body weight (Fig. S1G). Administration of PF-05231023 in alcohol-preferring vervet monkeys had no adverse effects on health or serum parameters (Table S1). Together, these data suggest that endogenous FGF21 signals in an endocrine fashion to regulate alcohol consumption while pharmacologic administration of FGF21 or FGF21 analogues can robustly suppress alcohol consumption in mice and alcohol-preferring primates.

FGF21 signals to KLB expressing neurons in the basolateral amygdala to suppress alcohol consumption.

FGF21 signaling to the brain is required for its ability to suppress alcohol consumption (Schumann *et al.*, 2016). However, the regional and cellular target(s) for FGF21 to suppress alcohol consumption is unknown. To identify central FGF21 target regions, we labeled KLB-expressing cells with the fluorescent protein tdTomato through viral delivery of a PHP.eB-FLEX-tdTomato virus (Chan et al., 2017) to KLB-Cre mice (Jensen-Cody *et*

al., 2020) (Fig. 2A). Importantly, the basolateral amygdala (BLA) exhibited defined and prominent expression of tdTomato (Fig. 2A). To investigate whether FGF21 signaling in the BLA may contribute to FGF21's suppression of alcohol consumption, we infused FGF21 or PF-05231023 directly into the BLA via unilaterally implanted cannula (Fig. 2B). Similar to IP administration of FGF21 (Fig. 1D), delivery of FGF21 (Fig. 2B) or PF-05231023 (Fig. 2C) to the BLA suppressed alcohol consumption in WT mice relative to littermate controls receiving vehicle infusions. Direct delivery of FGF21 or PF-05231023 to the BLA did not significantly change water consumption (Fig. S2A,B) or food intake (Fig. S2C,D) during the two-bottle choice with ethanol. To determine necessity of FGF21 signaling in the BLA for FGF21-mediated suppression of alcohol consumption, KLB was deleted in neurons in the BLA through delivery of AAV-hSyn-Cre or AAV-hSyn-EGFP to the BLA of $KLB^{fl/fl}$ mice (Fig. 2D). Deletion of KLB specifically in the BLA blocked the ability of IP administration of FGF21 to suppress alcohol consumption (Fig. 2E). In contrast, deletion of KLB in the BLA did not block FGF21's ability to suppress sucrose intake (Fig. S2E) which is consistent with previous work demonstrating that FGF21 signaling to the ventromedial hypothalamus is both sufficient and necessary for FGF21's effects to suppress carbohydrate preference (Jensen-Cody *et al.*, 2020).

To determine how FGF21 influences the excitability and activity of KLB^+ neurons in the BLA, we performed patch-clamp recordings in KLB^+ neurons in BLA brain slices after treatment with FGF21 in the presence of synaptic blockers. FGF21 application to brain slices significantly depolarized the resting membrane potential and increased membrane resistance in KLB^+ neurons in the BLA (Fig. 2F,G) indicating increased excitability of KLB^+ neurons following FGF21 administration. In support of this finding, FGF21 application increased the frequency of action potential firing in KLB^+ neurons in the BLA during current clamp recording (Fig. 2H, Fig. S2F). We next used single-cell RNA sequencing to investigate which cell types in the BLA express KLB and whether FGF21 treatment in vivo influences transcriptional profiles of KLB^+ BLA neurons. *Klb*-expressing cells represent multiple neuronal and non-neuronal populations in the BLA (Fig. 2I,J **and** Fig. S2G). In $KLB^+/Slc17a7^+$ neurons, FGF21 administration significantly enriched transcriptional programs associated with nervous system development and peptide metabolism in pre-synaptic glutamatergic compartments (Fig. 2K,L). These data suggest that FGF21 signals to KLB^+ neurons in the BLA to suppress alcohol consumption and can modulate neuronal function and peptide metabolism in KLB^+ glutamatergic neurons.

FGF21 preferentially influences excitability of $KLB^{BLA \rightarrow NAc}$ projection neurons and D2 MSNs in the NAc.

To determine downstream targets of BLA KLB^+ neurons, we performed anterograde tracing of KLB^+ neuron projections from the BLA by injecting AAV-hSyn-DIO-mCherry into the BLA of KLB-Cre mice and observed labeling of projection terminals in the nucleus accumbens (NAc) (Fig. 3A), a brain region strongly associated with integration of reward signaling and homeostatic dysregulation associated with substance use disorders. We did not observe labeling of projection terminals in other structures which BLA projections have been described including the hippocampus, pre-frontal cortex, and central amygdala (Fig. S3A). While we did observe projections in the bed nucleus of the stria terminalis

(BNST, Fig. S3A) it is unclear whether these projections are collaterals extending to the NAc. Multiple retrograde viral labeling strategies were used to confirm that a sub-population of KLB^{+} neurons in the BLA project to the NAc ($KLB^{BLA\rightarrow NAc}$, Fig. 3B, S3B). To determine whether in vivo administration of FGF21 influences the activity of $KLB^{BLA\rightarrow NAc}$ neurons, we performed patch-clamp experiments investigating excitability and action potential firing of $KLB^{BLA\rightarrow NAc}$ neurons compared to non-NAc projecting KLB^{+} neurons in the BLA (KLB^{BLA}) following three days of FGF21 administration (Fig. 3C). When evaluating the effect of FGF21 administration on excitability and action potential firing in $KLB^{BLA\rightarrow NAc}$ neurons in the presence of synaptic blockers, we observed an increase in excitability and action potential firing specifically in $KLB^{BLA\rightarrow NAc}$, but no effect in KLB^{BLA} neurons (Fig. 3D-G, S3C). These data suggest that FGF21 administration preferentially enhances excitability of $KLB^{BLA\rightarrow NAc}$ neurons while minimally affecting the excitability and firing properties of KLB^{BLA} neurons which project elsewhere. Classically, BLA→NAc projections are glutamatergic and regulate consummatory and reward-seeking behavior through excitatory neurotransmission onto medium spiny neurons (MSNs) in the NAc (Ambroggi et al., 2008; Beyeler et al., 2016; Millan et al., 2017; Namburi et al., 2015; Reed et al., 2018; Stefanik and Kalivas, 2013; Stuber et al., 2012; Stuber et al., 2011). To determine whether FGF21 administration influences glutamatergic inputs onto MSNs in the NAc, we recorded spontaneous excitatory post synaptic currents (sEPSC) in D1- and putative D2-expressing MSNs in the NAc of mice treated with vehicle or FGF21. We observed a specific potentiation of the frequency of sEPSCs in putative D2-MSNs but, not D1-MSNs (Fig. 3H-L). Thus, FGF21 increases the excitability and action potential firing of $KLB^{BLA\rightarrow NAc}$ neurons and facilitates glutamatergic input onto D2-MSNs in the NAc.

FGF21 and PF-05231023 suppress alcohol consumption by signaling through $KLB^{BLA\rightarrow NAc}$ projecting neurons.

Given the nature of FGF21's influence on glutamatergic signaling in the NAc and previous work suggesting that glutamatergic BLA→NAc projections influence reward seeking (Ambroggi *et al.*, 2008; Namburi *et al.*, 2015; Stefanik and Kalivas, 2013; Stuber *et al.*, 2011) and alcohol consumption (Millan *et al.*, 2017), we examined whether FGF21 signaling in $KLB^{BLA\rightarrow NAc}$ neurons contribute to FGF21's ability to suppress alcohol consumption. To do so, we used a dual recombinase strategy to restore endogenous expression of KLB specifically in BLA→NAc projecting populations. First, we used CRISPR to generate a mouse model in which endogenous β-klotho expression is prevented by a LoxP-flanked transcription blocker (loxTB) but can be reactivated by Cre recombinase (KLB loxTB) (Fig. 4A, S3D,E). Next, we administered a retrograde AAV-FLP-expressing virus in the NAc and an AAV-FLP-dependent Cre virus in the BLA, to express Cre and thus KLB specifically in BLA→NAc projecting neurons (Fig. 4B). Notably, while KLB loxTB/loxTB mice (KLB loxTB/$loxTB^{Ctrl}$) were completely refractory to the pharmacological effects of FGF21 or PF-05231023, restoration of KLB specifically to BLA→NAc projecting neurons (KLB loxTB/$loxTB^{BLA\rightarrow NAc}$) resulted in a significant suppression of alcohol consumption following administration of FGF21 or the FGF21 analogue PF-05231023, comparable to that of littermate controls (Fig. 4C-J). In contrast, restoration of *KLB* expression in BLA→NAc projecting neurons did not restore FGF21's ability to suppress sucrose consumption (Fig. 4K-N) or decrease body weight (Fig. S3F), suggesting that

FGF21 signaling to KLB$^{BLA\rightarrow NAc}$ neurons specifically regulates alcohol consumption. In summary, these data demonstrate that FGF21 signaling in KLB$^{BLA\rightarrow NAc}$ neurons is both necessary and sufficient to suppress alcohol consumption.

Discussion

These findings identify a homeostatic liver-to-brain circuit which regulates alcohol consumption and demonstrate the feasibility of targeting this pathway for therapeutic applications. Specifically, FGF21 signaling in BLA→NAc projecting neurons suppresses alcohol consumption by enhancing the excitability of a specific subpopulation of these neurons. The association of increased FGF21 levels with alcohol consumption and alcohol liver cirrhosis (Wagner-Skacel *et al.*, 2021) may suggest a pathology in this pathway contributes to alcohol dependency. Importantly, FGF21 and the FGF21 analogue, PF-05231023, effectively function to decrease alcohol intake even when administered after prolonged ethanol exposure in mice and primates. In addition, both maintain their potency in rodent models of excessive alcohol consumption such as intermittent access, and PF-05231023 decreases ethanol consumption in primates which exhibit a strong innate preference for ethanol. Thus, FGF21 based therapeutics may represent a promising therapeutic approach for AUD.

In addition to effects on ethanol consumption, we have previously demonstrated that FGF21 suppresses sugar intake via a liver-to-brain signaling axis (Jensen-Cody *et al.*, 2020). We demonstrate here that FGF21 suppresses alcohol consumption through a distinct circuit from the one(s) mediating FGF21's effects on sugar intake (Jensen-Cody *et al.*, 2020). Thus, FGF21 appears to be an endocrine protective factor that signals to specific, non-overlapping central neural circuits to prevent nutrient excess and associated liver damage. When considering how and why these modality specific mechanisms evolved, it is interesting to note that mammals were primarily exposed to alcohol from fermenting fruits, which possess high levels of simple sugars. Despite this, neural circuits regulating FGF21-mediated suppression of sugar and alcohol intake apparently developed independently and not in response to a shared selective pressure.

A previous study reported that FGF21 increases water intake "or thirst" in mice presented with alcohol (Song et al., 2018). Instead, we find that FGF21 signaling in the BLA suppresses alcohol intake without significantly altering water intake in mice. In addition, PF-05231023 did not affect water consumption in alcohol preferring vervet non-human primates. We also previously found that FGF21 administration does not acutely increase total fluid intake in a two-bottle choice assay with or without sucrose (Flippo et al., 2020). Importantly, physiological plasma FGF21 levels are not significantly altered by hydration status (Carroll et al., 2020). We instead hypothesize that observed effects of FGF21 on water intake in mice may occur secondarily to FGF21's effects on energy expenditure (Camporez et al., 2013) and prandial thirst (BonDurant and Potthoff, 2018). Nevertheless, while the effects of FGF21 to suppress alcohol intake functions through signaling in the BLA, the effect of FGF21 on body weight reduction and any potential effect on water intake, are independent of FGF21 signaling to the BLA.

Prolonged FGF21 administration influences dopamine levels in mesolimbic circuitry but it was unclear whether this effect was direct or indirect (Talukdar *et al.*, 2016a). Our findings here provide additional context to this data and suggest that FGF21 is not acting directly on mesolimbic circuitry to suppress alcohol consumption but instead through modulatory inputs to the NAc via $KLB^{BLA\rightarrow NAc}$ neurons. BLA→NAc projections have been reported to contribute to regulation of reward-seeking and consummatory behavior (Ambroggi *et al.*, 2008; Millan *et al.*, 2017; Namburi *et al.*, 2015; Reed *et al.*, 2018; Stefanik and Kalivas, 2013; Stuber *et al.*, 2011). However, BLA→NAc projections appear to have opposing effects on reward-seeking and consummatory behavior. For example, while optogenetic excitation of BLA→NAc projections promotes reward seeking behavior (intracranial self-stimulation) (Folkes et al., 2020; Namburi *et al.*, 2015; Stuber *et al.*, 2011), similar optogenetic excitation suppresses ethanol and sucrose consumption (Millan *et al.*, 2017). Furthermore, optogenetic inhibition of BLA→NAc projections has been reported to promote consummatory behavior (Reed *et al.*, 2018). In this study, we find that FGF21 administration enhances excitability of $KLB^{BLA\rightarrow NAc}$ neurons and suppresses alcohol consumption supporting data that excitation of BLA→NAc projections is capable of suppressing alcohol consumption. FGF21's effects on consummatory behavior through BLA→NAc projections appears specific to ethanol as sucrose and chow consumption are unaffected by FGF21 signaling in the BLA and BLA→NAc projections. One interpretation of these findings suggests that sub- populations of BLA→NAc projections facilitate distinct behavioral outcomes through distinct output targets in the NAc (rostral vs. caudal, D1 vs. D2, etc.). Our work indicates that FGF21 specifically alters excitability of D2 MSNs but not D1 MSNs, and we therefore propose a model wherein $KLB^{BLA\rightarrow NAc}$ neurons represent a sub-population of BLA→NAc projecting neurons which specifically regulate ethanol consumption through effects on excitability of D2 MSNs in the NAc. Additionally, FGF21 administration may influence other aspects of $KLB^{BLA\rightarrow NAc}$ neuron function beyond excitability to contribute to suppression of alcohol consumption. Overall, our work demonstrates the existence of an endocrine sensitive subpopulation of amygdalo-striatal projecting neurons which powerfully suppress alcohol consumption when excited by the liver-derived, endocrine hormone FGF21 or FGF21 analogues. Thus, these results provide a mechanism for a liver-to-brain endocrine feedback loop which presumably functions to protect the liver from damage. The central molecular and cellular effects of FGF21 represent an opportunity for future research and the present data indicates that FGF21 analogues may provide a potential treatment option against AUD and related diagnosis.

Limitations of the Study

We find that FGF21 alters glutamatergic input to putative D2 MSNs in the NAc and requires KLB expression in BLA→NAc projecting neurons to suppress alcohol consumption. Further investigation is required to determine whether FGF21 mediates effects on glutamatergic transmission in the NAc through signaling to BLA→NAc projecting neurons. Additionally, while we demonstrate that *in vivo* administration of FGF21 increases action potential firing in $KLB^{BLA\rightarrow NAc}$ neurons in acute brain slices, the specific effects of FGF21 on activity of $KLB^{BLA\rightarrow NAc}$ neurons *in vivo* during alcohol consumption require future exploration.

STAR Methods

Resource Availability

Lead contact—Matthew J. Potthoff, matthew-potthoff@uiowa.edu

Materials Availability—All unique/stable reagents generated in this study are available from the Lead Contact.

Data and Code Availability—RNA sequencing data is available in the NCBI Gene Expression Omnibus (GEO) and Sequence Read Archive (SRA) under accession number GEO: GSE######. Further requests for data are available upon correspondence with the Lead Contact.

Experimental model and subject details

All mouse experiments presented in this study were conducted according to the animal research guidelines from NIH and were approved by the University of Iowa IACUC. All non-human primate experiments were conducted at the St Kitts laboratories of Behavioral Science Foundation (BSF). All experiments were reviewed and approved by the BSF Institutional Animal Care and Use Committee (BSF IACUC), operating under the auspices of the Canadian Council on Animal Care (Canadian Council on Animal Care Good Animal Practice registration A5028) and all of the procedures used in the study were covered by standard operating procedures approved by the BSF IACUC (BSF 1906). Thirty-two young adult, male vervet monkeys (*Chlorocebus sabaeus*) (body weight: 4.1–6.3 kg) were used in total. Alcohol intake was screened in all subjects prior to use in any experiments. Subjects had not been used in any prior experiments.

Animals—The following mice utilized in these studies have been previously described (Jackson stock number in parenthesis): $FGF21^{fl/fl}$ (Markan *et al.*, 2014), FGF21 LivKO (Markan *et al.*, 2014), $KLB^{fl/fl}$ (Ding *et al.*, 2012), Ai14-tdTomato (007914), and KLB-Cre (Jensen-Cody *et al.*, 2020). KLB loxTB mice were generated for this study at the Iowa Genome Editing Facility using CRISPR/Cas9 to insert a floxed transcriptional blocking sequence (an En2 splice acceptor followed by three SV40 poly-A sequences) in the intronic region between exon 1 and exon 2 of *Klb*. Proper insertion was confirmed by sequencing of the genomic locus. All mice used in experiments were individually housed under a 12 hr light/dark cycle at room temperature (21–23°C). Littermates of the same sex were randomly assigned to experimental groups. All animals used for behavioral experiments in this study were between 12–16 weeks of age at the initiation of experiments. All animals were used in scientific experiments for the first time. This includes no previous exposures to pharmacological substances. All mice were on a C57BL6/J genetic background except for the KLB loxTB mice which were on a mixed background (C57BL6/129Sv). Chow diets were provided to all mice used in this study (Teklad 2920x). Health status was normal for all animals. Mice for electrophysiology experiments recording from the nucleus accumbens were aged 8–10 weeks and housed together in groups of five per cage on a 12/12 hour light/dark cycle and housed at Vanderbilt University Medical Center. C57BL/6J mice were

bred to carry a bacterial artificial chromosome expressing the tdTomato fluorophore under the control of the *Drd1a* promoter.

Method details

AAV-TBG administration—For AAV-TBG injections, $FGF21^{fl/fl}$ mice were anesthetized with 3% isoflurane and retro-orbitally injected with 10 μl of AAV8-TBG-PI-Cre (8×10^{12} vg/ml, Addgene #: 107787-AAV8) or AAV8-TBG-PI-Null (8×10^{12} vg/ml, Addgene #: 105536-AAV8) in a total volume of 100 μl saline. These viruses were a gift from James M. Wilson (Addgene viral prep # 107787-AAV8 and 105536-AAV8). Mice were allowed to recover for 4 weeks post-surgery to allow for viral expression and recombination of floxed *Fgf21* before being used for experiments.

Plasma Analysis—Blood was collected from the tail vein into 300K2E microvettes (Sarstedt) and spun at 3000 rpm for 30 min at 4°C to separate plasma. Mouse FGF21 was measured using a commercially available ELISA (Biovendor) based on the manufacturer's instructions. During analysis of the ELISA data the blank values were subtracted from the experimental values to account for non-specific absorbance detected in the plate wells. Plasma ethanol (EtOH) concentrations were determined using a commercially available kit (EnzyChrom). In both cases the manufacturer's instructions were followed to quantify the analytes.

EtOH Gavage—For three days prior to the experiment mice were gavaged with water to de-sensitize them to the gavage process. On the day of the experiment a pre-gavage sample of blood was collected prior to gavage with 3.5g/kg EtOH in water. Blood samples were then processed as described above.

IP administration of FGF21 and PF-05231023 in mice—Recombinant human FGF21 was generated and provided by Novo Nordisk. For consumption studies, mice received daily intraperitoneal (IP) injections of vehicle or FGF21 at 1 mg/kg and were put back in home-cages with access to fluid solutions. PF-05231023 was generated and provided by Pfizer and mice received a single IP injection of PF-05231023 at 10 mg/kg every four days for the 2-BC experiment and 3 mg/kg every four days for the IA experiment and were put back in home-cages with access to fluid solutions.

Two-Bottle Choice Experiments—For two-bottle choice experiments, drinking tubes were constructed and fluids were presented following the Monell Mouse Taste Phenotyping Project specifications (http://www.monell.org/MMTPP/), and mice were offered ad libitum consumption of the tested fluid (ethanol (EtOH) or sucrose) versus water. Fluid solution positions were switched every three days to prevent potential bottle placement bias. Solutions were available 24h/day and fluid intake was recorded daily. Solutions were prepared with tap water and served at room temperature. The spillage from drinking tubes was estimated daily by recording the change in fluid levels of two drinking tubes that were placed on an empty cage where one tube contained that day's test solution, and the other tube contained water.

Intermittent access experiments—The intermittent access experiments were performed as described (Hwa *et al.*, 2011). Briefly, mice were allowed access to ethanol for 24 hours on the first, third, and fifth day of each week. On days 1 and 4 of each week, mice were administered vehicle or PF-05231023 (3mg/kg, IP) until the indicated washout period during which no PF-05231023 was administered.

Administration of PF-05231023 in non-human primates

Subjects and Housing: Vervet monkeys were well-acclimated and born in the colony at the Behavioral Science Foundation (BSF), Saint Kitts. Prior to initiating an experiment, subjects were socially housed in large outdoor wire cages as described (26). Monkeys were maintained on a high protein diet (Teklad Global 20% Protein Primate Diet (2055); Harlan Teklad, Madison, WI) and fresh local produce. Water was available ad libitum.

During screening periods and experiments, alcohol ingestion was assessed in singly housed subjects that were always in visual and olfactory contact with one another. Experiments were performed January to February (study 1; typical ambient temperature 28 ° C) and in July to August (study 2; temperature 31 ° C).

Alcohol Preference Screening: Animals to be screened for alcohol preference were moved from their group cages and housed individually in a roofed, outdoors area close to the group cages. Following one day of habituation to housing, each animal was presented with a two-bottle choice paradigm, in which one bottle contains 10% w/v ethanol in tap water and the other contains only tap water. These bottles were available 24 h/d for 5 days (water was replenished as needed), followed by 5 days of 4 h access. Alcohol consumption was calculated as g/kg/day, and alcohol preference was calculated as a ratio of alcohol vs total liquid consumed. Throughout this period, water was available ad libitum, and animals were always in visual and olfactory communication with one another. Animals consuming 3 g/kg/day were included in these studies.

Safety Study: A pilot study to evaluate safety of the study drug (approval number BSF 1904) was conducted. Three healthy adult males were each administered 3 doses (1 mg/kg, 2 mg/kg, 5 mg/kg) of the test article on successive Tuesday mornings. Animals were observed 2, 4, 6 and 8 h after administration and again at 8 am the following morning, with particular attention to signs of nausea, reduced food or water intake, and diarrhea or other fecal anomalies.

Placebo controlled study: Subjects (n = 20) were allowed a choice between a 10% (w/v) alcohol solution and water for 4 h/day for five days per week. After establishing a baseline over nine days, monkeys were randomly placed into either a placebo (n = 8) or treatment (n = 12) group. At this time, subjects were anesthetized and administered intravenously either saline or PF-05231023 (1 mg/kg) once per week (Mondays). For drug administration and blood sampling, monkeys were cage squeezed and anesthetized with ketamine subcutaneously where after drug was administered or 2 mL of whole blood were drawn from the femoral vein. During the experiment, monkeys were observed for possible side effects (e.g., vomiting, reduced food intake, weight loss or skin irritation at the injection

sites). After two four-day periods in which two doses of 1 mg/kg were administered, the dose was increased to 2 mg/kg for an additional two four-day periods. After the last administration at 2 mg/kg, a washout period was performed for two four-day periods. Weights were measured at the start, middle and end of the study.

Plasma Analysis: A few days after the drug was administered, blood was drawn after a 4-hour period in which monkeys had access to water and alcohol. Two aliquots of blood were prepared as plasma using either EDTA or potassium oxalate/sodium fluoride. EDTA plasma was used for the measurement of albumin, alkaline phosphatase, ALT, amylase, AST, BUN, calcium, cholesterol, creatinine phosphokinase, chloride, creatinine, gamma glutamyl transferase, globulin, glucose, potassium, sodium, phosphorus, total bilirubin, total protein, triglycerides. Potassium oxalate/sodium fluoride plasma was used for the measurement of alcohol. All measurements were performed by VRL (San Antonio, Texas, USA).

Statistical Analysis: A repeated measure, two-way ANOVA was performed to detect effects of time, treatment, and an interaction thereof. The washout period was not included in the analysis of alcohol ingestion or water intake. False discovery rate ($q < 0.05$) corrected multiple comparisons were performed to compare treatment to placebo at each time point using the two-stage linear step-up procedure of Benjamini, Krieger and Yekutieli. Comparisons between the washout periods at each time point were performed with FDR corrected (two-stage linear step-up procedure of Benjamini, Krieger and Yekutieli, FDR = 1%) multiple comparisons. Baselines in all studies were compared using a one-way ANOVA. An alpha level of 0.05 was considered significant. Data is displayed as mean ± standard error of the mean (SEM).

PHP.eB administration—For PHP.eB injections, mice were anesthetized with 3% isoflurane and retro-orbitally injected with 10 μl of the following viruses: pAAV-FLEX-tdTomato (8×10^{12} vg/ml, Addgene #: 28306), PHP.eb-GFP (8×10^{12} vg/ml, Addgene #: 37825). Mice were allowed to recover for 4 weeks post-surgery to allow for proper viral spread, and brains were collected and processed for experiments.

Surgery—Adult mice (8–12 weeks old) were anesthetized with 2%−3% isoflurane and placed on a stereotaxic frame. Heat pads were used through the duration of the surgery to keep the body temperature stable. Eye ointment was applied to keep the eyes from drying. An incision was made to the skin to expose the skull after asepsis with Betadine and medical alcohol was applied. For viral injection, a craniotomy was made and a 1 μL Hamilton Neurosyringe 7100 was slowly inserted into the target region. 0.5–1 μl of virus ($\geq1\times10^{13}$ vg/ml) was injected with an injection speed of 0.10 ul per minute. The following coordinates were used for injection into the listed brain regions; basolateral amygdala (BLA, AP −1.38, ML +/−3.00, DV −4.46), nucleus accumbens (NAc, AP +1.34; ML +/− 0.75; DV −4.55). Animals recovered for at least 4 weeks after surgery to allow for viral expression.

AAV viral constructs—The following viral constructs were used in this study; AAV-hSyn-HI-eGFP-Cre (Addgene #: 105540-AAV9), AAV-hSyn-EGFP (Addgene #: 50465-AAV9), AAV-hSyn-DIO-mCherry (Addgene #: 50459-AAV9 and AAVrg), AAV-hSyn-DIO-

EGFP (Addgene #: 50457-AAVrg), AAV-EF1a-Flpo (Addgene #: 55637-AAVrg), AAV-EF1a-fDIO-Cre (Addgene #: 121675-AAV9).

Cannula implantation—A similar surgical protocol as described above was used to implant cannula unilaterally into the BLA. Cannula were secured to the skull with stainless steel screws and dental cement. Animals were allowed to recover for at least 1 week after surgery. Drug infusions were administered using an internal cannula (33-gauge) that extended 1mm beyond the tip of the cannula over a period of 5 minutes in a final volume of 1 μL.

Gene Expression—Gene expression analyses were performed as described[36]. RNA was isolated from brain tissue following Trizol (Invitrogen) protocol and a Direct-zol RNA MiniPrep plus kit (Zymo Research). 2 μg of RNA from each sample was used to generate cDNA (High-Capacity cDNA Reverse Transcription Kit; Life Technologies), and QPCR was conducted using SYBR green (Invitrogen). QPCR primer sequences are as follows: *Klb*: 5' -GATGAAGAATTTCCTAAACCAGGTT −3', 5' -AACCAAACACGCGGATTTC −3'; *U36B4*: 5'-CGTCCTCGTTGGAGTGACA-3', 5'- CGGTGCGTCAGGGATTG-3'; *Fgf21*: 5'-CCTCTAGGTTTCTTTGCCAACAG-3', 5'- AAGCTGCAGGCCTCAGGAT-3'; *Cre*: 5'-TGTTGCCGCGCCATCTG-3', 5'- TTGCTTCAAAAATCCCTTCCA-3'.

Single-Cell RNA-Sequencing—Generation of single cell suspensions

The method used here for generating single cell suspensions was modified from a previously published protocol (Wu et al., 2017). Individual mice were quickly decapitated, the brain was immediately extracted and placed in fresh ice-cold artificial cerebrospinal fluid (aCSF) containing 124 mM NaCl, 2.5 mM KCl, 1.2 mM NaH_2PO_4, 24 mM $NaHCO_3$, 5 mM HEPES, 13 mM glucose, 2 mM $MgSO_4$, and 2 mM $CaCl_2$, bubbled with a carbogen gas (95% O_2 and 5% CO_2) and with a pH of 7.3 – 7.4. Brains were then sectioned on a vibratome and sections containing the BLA were placed in ice cold aCSF w/actinomycin D (93 mM N-methyl-D-glucamine, 2.5 mM KCl, 1.2 mM NaH2PO4, 30 mM NaHCO3, 20 mM HEPES, 25 mM glucose, 10 mM MgSO4, 0.5 mM CaCl2, 5 mM sodium ascorbate, 2 mM thiourea, and 3 mM sodium pyruvate, 45 μM actinomycin D, pH of 7.3–7.4, bubbled with carbogen gas (95% O2 and 5% CO2) on ice for at least 15 minutes prior to dissection). The BLA was then dissected from each section, and BLA tissue derived from three mice were pooled for each experimental condition. The tissue was then minced and placed in 2mg/ml Pronase in aCSF w/actinomycin D and incubated at 37°C for 30 minutes. Following digestion, the Pronase solution was exchanged with ice-cold, carbogen-bubbled ACSF containing 1% fetal bovine serum and .01% BSA. The tissue was then titrurated using fire polished Pasteur pipets and strained through a 70 μM cell strainer.

FACS sorting: FACs sorting for tdTomato positive cells was performed as previously described (Jensen-Cody *et al.*, 2020). Hoechst cell viability dye (Hoechst 33258) was added to the cell suspension at a final dilution of 4ug/ml just prior to sorting to allow for selection of living cells during FACs sorting. Cells were then FACs sorted for tdTomato fluorescence and viability via Hoechst staining. Sorting was performed on a BD FACS Aria II using a

130 mM nozzle, a sheath pressure of 10 p.s.i., and in the single cell sorting mode at the University of Iowa Flow Cytometry Facility.

Single cell capture and cDNA library construction: FACS isolated cells were then loaded on the BD Rhapsody where capture of the single cells was performed per manufacturer instructions. Following lysis of the cells and capture of mRNA on oligonucleotide barcoded beads the cDNA synthesis was performed and cDNA libraries with Illumina sequencing adapters were generated per manufacturer instructions using the BD Rhapsody whole transcriptome analysis amplification kit. cDNA libraries were then sequenced on Illumina HiSeq 4000 sequencers at the University of Iowa Genomics Core. Sequencing data was then quality filtered and annotated using the BD Rhapsody analysis pipeline while also correcting for artifacts which arise during library construction. Filtered and annotated data from vehicle and FGF21 treated mice were then normalized in the R package Seurat using SCTransform and integrated using Seurat scRNA-seq integration (Stuart et al., 2019). Imputation was performed using the Seurat Wrapper ALRA on the integrated data set before final clustering (clustering resolution was set at 0.5 based on the number of cells sequenced)(Table S2) and gene expression analysis to account for dropout associated with 3'-barcoding-based approaches (Ziegenhain et al., 2017). "Cell type" classification of the clusters was determined based on expression of previously identified marker genes for neuronal and non-neuronal cell types.

Immunohistochemistry—For immunohistochemistry, mice were anesthetized and transcardially perfused using 25 mL PBS followed by 25 mL 4% paraformaldehyde (PFA). Brains were collected and post fixed for 24 hours in 4% PFA and transferred to a 30% sucrose for at least 48 hours. Brains were cryoprotected in Tissue-Tek optimal cooling temperature (OCT) compound and stored in a −80 freezer until use. 40 μm coronal sections were cut using a Leica cryostat. Brain slices were washed and permeabilized with PBST (0.4% Triton X-100 in PBS) over 15 minutes and incubated with blocking solution (5% normal goat serum in PBST) for 1 hour at room temperature. Slices were incubated in rabbit α-HA-tag (1:1000, Cell signaling: 3724S) overnight at 4°C. The following day slices were washed in PBST over 15 minutes and incubated in the AlexaFluor488-fluorescently-conjugated goat anti-rabbit secondary (1:250, Life Technologies) at RT for 1 hour. Finally, slices were mounted on slides with VECTASHIELD Antifade Mounting Media with DAPI (Vector Laboratories). Slices were imaged using Leica SPE Confocal Microscope maintained by the Iowa Neural Circuits and Behavioral Core.

Electrophysiology for BLA recordings—Slice preparation was performed as described previously (Jensen-Cody *et al.*, 2020). Briefly, 8-week old KLB-Cre or KLB-Cre::Ai14-tdTomato mice infected with PHP.eB-DIO-tdTomato virus or AAV-rgDIO-GFP into the NAc, respectively, and were sacrificed and brains were immersed in NMDG-HEPES aCSF cutting solution (in mM): 92 NMDG, 2.5 KCl, 1.25 NaH_2PO_4, 30 $NaHCO_3$, 20 HEPES, 25 glucose, 2 thiourea, 5 Na-ascorbate, 3 Na-pyruvate, 0.5 $CaCl_2 \cdot 2H_2O$, and 10 $MgSO_4 \cdot 7H_2O$). Brain tissue is kept in 95% O_2 / 5% CO_2 aerated ice-cold cutting solution and 300 μm thick fresh slices containing the BLA were obtained with vibratome and transferred to 95% O_2 / 5% CO_2 aerated and HEPES containing aCSF incubation solution

containing (in mM): 92 NaCl, 2.5 KCl, 1.25 NaH2PO4, 30 NaHCO3, 20 HEPES, 25 glucose, 2 thiourea, 5 Na-ascorbate, 3 Na-pyruvate, 2 CaCl2·2H2O, and 2 MgSO4·7H2O. The sections were incubated in this solution for at least 30 minutes and placed in the recording chamber which has the recording aCSF (in mM): 124 NaCl, 2.5 KCl, 1.25 NaH2PO4, 24 NaHCO3, 12.5 glucose, 5 HEPES, 2 CaCl2·2H2O, and 2 MgSO4·7H2O. Loose seal recordings are performed using aCSF in pipette and action currents are monitored in the presence of a cocktail of synaptic blockers CNQX (10 μM) + AP5 (50 μM) + PTX (50 μM). Whole cell recordings were performed in current clamp mode and membrane voltage were recorded from tdTomato$^+$- and tdTomato$^+$/GFP$^+$-expressing KLB$^+$ BLA neurons using electrodes with 4–5 MΩ tip resistances in the presence of synaptic blockers. Pipette solution contained (in mM): 145 K-gluconate, 1 MgCl2, 10 HEPES, 1.1 EGTA, 2 Mg-ATP, 0.5 Na2-GTP, and 5 Na2-phosphocreatine (pH 7.3 with KOH; 290–295 mOsm). Recordings were corrected for liquid junction potential. Current injection protocol was set for 300 ms pulses of 30 pA (or 50 pA) steps starting from 150 pA to +150 pA (or 300 pA). MultiClamp 700B Amplifier (Molecular Devices, San Jose, CA) and Axon pCLAMP 11.3 software (Molecular Devices, San Jose, CA) were used to obtain and analyze data. Vm was monitored before and after administration of FGF21 (50 ng/μl) into the bath through perfusion or in brain slices from mice treated with vehicle or FGF21 for 3 days prior. Overall Rm was calculated by analyzing the hyperpolarizing voltage deflection in response to current injection protocol of 300 ms pulses of 50 pA steps starting from 150 pA and using steady state portion of the pulses. Rm values at the resting membrane potential was calculated at voltage clamp mode using the steady state current in response to 10 mV of depolarizing voltage pulse for 100 ms.

Electrophysiology for NAc recordings—Whole-cell voltage-clamp recordings of neural transmission were collected from 8–10 week old Drd1a tdTomato mice. Mice were sacrificed under isoflurane anesthesia, brains were removed and placed in oxygenated (95% O_2, 5% CO_2), ice cold N-methyl-D-glucamine (NMDG) cutting solution (in mM: 2.5 KCL, 20 HEPES, 1.2 NaH_2PO_4, 25 glucose, 93 NMDG, 30 $NaHCO_3$, 5 sodium ascorbate, 3 sodium pyruvate, 10 $MgCl_2$ and 0.5 $CaCl_2 2H_2O$). 250 μM sagittal slices were taken using a Leica VT1200S Vibratome. Slices were recovered at 32˚ C for 10 minutes before being transferred to chambers containing oxygenated artificial cerebrospinal fluid (ACSF; in mm: 119 NaCl, 2.5 KCl, 1.3 MgCl2–6H2O, 2.5 CaCl2–2H2O, 1.0 NaH2PO4-H2O, 26.2 NaHCO3, and 11 glucose). Experiments were performed using a Scientifica SliceScope Pro system while continuously perfused with 30˚ C +/− 2˚ ACSF at 2ml/min. Neurons in the lateral NAc core were visualized using Scientifica PatchVision software and patched with 3–4 MΩ recording pipettes (made with a P1000 Micropipette puller) filled with a cesium (Cs^+)-based internal solution (in mM: 120 CsMeSO3, 15 CsCl, 8 NaCl, 10 HEPES, 0.2 EGTA, 10 tetraethylammonium (TEA)-Cl, 4.0 Mg-ATP, 0.3 Na-GTP, 0.1 spermine, and 5.0 QX 314 bromide).

Drd1a positive and Drd1a negative MSNs were differentiated according to the expression of the tdTomato flurophore via 530 nm LED light. MSNs were differentiated from interneuron cell types based on morphology (size, shape) and biophysical properties (capacitance, membrane resistance, and AMPAR decay kinetics). Slices containing nucleus accumbens core were identified primarily by the morphology of the anterior commissure and all cells

sampled were located dorsally within the accumbens near the commissure to avoid lateral accumbens shell. Cells were voltage clamped at −70 mV and sEPSCs were collected for 5 minutes following a 5-minute equilibration time after break in. sEPSC analysis was performed with Clampfit 10.4 using a best- fit template obtained from preliminary recordings from NAc MSNs. Execution of experimental protocols and data collection were accomplished using Molecular Devices pClamp 10 Analysis software. Monitoring electrical properties of cells was achieved using AxoPatch 500B Multiclamp amplifier and Axon Digidata 1550 low-noise data acquisition digitizer. Responses were filted at 2 kHz and digitized at 10 kHz.

Quantification and statistical analysis: Sample sizes for experiments were determined based on sample sizes used in similar experiments reported previously in the literature. Statistical analysis was conducted using GraphPad Prism software in which distribution of the data was analyzed to determine the appropriate statistical test to be applied. The statistical test used for each comparison is described in the figure legends corresponding to the specific figure. Data are presented as the mean ± SEM unless otherwise noted with $P < 0.05$ being the cut-off for a result to be considered significant. ‘‘n’’ corresponds to the number of individual mice or neurons analyzed as indicated. Read quality filtering for single-cell RNA sequencing was performed on paired-end reads to exclude sequencing reads with lengths 0.54 for R1 or >.79 for R2 prompted exclusion of the read pair. Only reads which passed all three quality filters were annotated and used to determine putative cells and quantify unique molecular identifiers for each cell. For fluid intake studies, mice were randomly assigned to groups. To determine whether data analyzed was normally distributed we employed QQ plots and the D’Agostino-Pearson test. To determine the variance in different experimental groups the F test was used when comparing two groups and the Bartlett’s test was used when comparing 3 or more groups. When the variance of data sets compared was not homogenous Welch’s test was employed to compare the groups.

Supplementary Material

Refer to Web version on PubMed Central for supplementary material.

Acknowledgments

We thank Dr. Birgitte Andersen (Novo Nordisk) for providing FGF21 protein. We thank Pfizer for providing PF-05231023. This work was funded by the National Institutes of Health (NIH) R01DK106104 (M.J.P.), R01AA027654 (M.J.P.), T32 DK112751 (K.H.F.), Brain Behavior Research Foundation Young Investigator Award 28026 (K.H.F.), F32 DK117510 (K.E.C.), F31 DK117515 (S.O.J.), and DK126740 (D.A.); Veterans Affairs Merit Review Program I01BX004634 (M.J.P.); the University of Iowa Carver College of Medicine (M.J.P.); the Novo Nordisk Foundation Center for Basic Metabolic Research (NNF18CC003490; M.P.G.); the Danish Council for Independent Research (0134–00375B); and the Novo Nordisk Foundation Metabolite Consortium (0064142). Some of the data presented herein were obtained at the Flow Cytometry Facility supported by the NIH (1 S10 OD016199–01A1). The authors would like to acknowledge the University of Iowa Central Microscopy Research Facility and Genome Editing Facility, the Genomics Division of the Iowa Institute of Human Genetics, and the Iowa Neuroscience Institute Neural Circuits and Behavior Core. Some figures included illustrations made using BioRender.com.

References

Adams AC, Cheng CC, Coskun T, and Kharitonenkov A (2012). FGF21 requires betaklotho to act in vivo. PLoS One 7, e49977. 10.1371/journal.pone.0049977.

Ambroggi F, Ishikawa A, Fields HL, and Nicola SM (2008). Basolateral amygdala neurons facilitate reward-seeking behavior by exciting nucleus accumbens neurons. Neuron 59, 648–661. 10.1016/j.neuron.2008.07.004. [PubMed: 18760700]

Ameka M, Markan KR, Morgan DA, BonDurant LD, Idiga SO, Naber MC, Zhu Z, Zingman LV, Grobe JL, Rahmouni K, and Potthoff MJ (2019). Liver Derived FGF21 Maintains Core Body Temperature During Acute Cold Exposure. Sci Rep 9, 630. 10.1038/s41598-018-37198-y. [PubMed: 30679672]

Beyeler A, Namburi P, Glober GF, Simonnet C, Calhoon GG, Conyers GF, Luck R, Wildes CP, and Tye KM (2016). Divergent Routing of Positive and Negative Information from the Amygdala during Memory Retrieval. Neuron 90, 348–361. 10.1016/j.neuron.2016.03.004. [PubMed: 27041499]

BonDurant LD, and Potthoff MJ (2018). Fibroblast Growth Factor 21: A Versatile Regulator of Metabolic Homeostasis. Annu Rev Nutr 38, 173–196. 10.1146/annurev-nutr-071816-064800. [PubMed: 29727594]

Camporez JP, Jornayvaz FR, Petersen MC, Pesta D, Guigni BA, Serr J, Zhang D, Kahn M, Samuel VT, Jurczak MJ, and Shulman GI (2013). Cellular mechanisms by which FGF21 improves insulin sensitivity in male mice. Endocrinology 154, 3099–3109. 10.1210/en.2013-1191. [PubMed: 23766126]

Carroll HA, Chen YC, Templeman I, James LJ, Betts JA, and Trim WV (2020). The effect of hydration status on plasma FGF21 concentrations in humans: A subanalysis of a randomised crossover trial. PLoS One 15, e0235557. 10.1371/journal.pone.0235557.

Chan KY, Jang MJ, Yoo BB, Greenbaum A, Ravi N, Wu WL, Sanchez-Guardado L, Lois C, Mazmanian SK, Deverman BE, and Gradinaru V (2017). Engineered AAVs for efficient noninvasive gene delivery to the central and peripheral nervous systems. Nat Neurosci 20, 1172–1179. 10.1038/nn.4593. [PubMed: 28671695]

Clarke TK, Adams MJ, Davies G, Howard DM, Hall LS, Padmanabhan S, Murray AD, Smith BH, Campbell A, Hayward C, et al. (2017). Genome-wide association study of alcohol consumption and genetic overlap with other health-related traits in UK Biobank (N=112 117). Mol Psychiatry 22, 1376–1384. 10.1038/mp.2017.153. [PubMed: 28937693]

Desai BN, Singhal G, Watanabe M, Stevanovic D, Lundasen T, Fisher FM, Mather ML, Vardeh HG, Douris N, Adams AC, et al. (2017). Fibroblast growth factor 21 (FGF21) is robustly induced by ethanol and has a protective role in ethanol associated liver injury. Mol Metab 6, 1395–1406. 10.1016/j.molmet.2017.08.004. [PubMed: 29107287]

Ding X, Boney-Montoya J, Owen BM, Bookout AL, Coate KC, Mangelsdorf DJ, and Kliewer SA (2012). betaKlotho is required for fibroblast growth factor 21 effects on growth and metabolism. Cell Metab 16, 387–393. 10.1016/j.cmet.2012.08.002. [PubMed: 22958921]

Edenberg HJ, and Foroud T (2013). Genetics and alcoholism. Nat Rev Gastroenterol Hepatol 10, 487–494. 10.1038/nrgastro.2013.86. [PubMed: 23712313]

Ervin FR, Palmour RM, Young SN, Guzman-Flores C, and Juarez J (1990). Voluntary consumption of beverage alcohol by vervet monkeys: population screening, descriptive behavior and biochemical measures. Pharmacol Biochem Behav 36, 367–373. 10.1016/0091-3057(90)90417-g. [PubMed: 2356209]

Flippo KH, Jensen-Cody SO, Claflin KE, and Potthoff MJ (2020). FGF21 signaling in glutamatergic neurons is required for weight loss associated with dietary protein dilution. Sci Rep 10, 19521. 10.1038/s41598-020-76593-2.

Flippo KH, and Potthoff MJ (2021). Metabolic Messengers: FGF21. Nat Metab 3, 309–317. 10.1038/s42255-021-00354-2. [PubMed: 33758421]

Folkes OM, Baldi R, Kondev V, Marcus DJ, Hartley ND, Turner BD, Ayers JK, Baechle JJ, Misra MP, Altemus M, et al. (2020). An endocannabinoid-regulated basolateral amygdala-nucleus accumbens circuit modulates sociability. J Clin Invest 130, 1728–1742. 10.1172/JCI131752. [PubMed: 31874107]

Haass-Koffler CL, Akhlaghi F, Swift RM, and Leggio L (2017). Altering ethanol pharmacokinetics to treat alcohol use disorder: Can you teach an old dog new tricks? J Psychopharmacol 31, 812–818. 10.1177/0269881116684338. [PubMed: 28093021]

Hsuchou H, Pan W, and Kastin AJ (2007). The fasting polypeptide FGF21 can enter brain from blood. Peptides 28, 2382–2386. 10.1016/j.peptides.2007.10.007. [PubMed: 17996984]

Hwa LS, Chu A, Levinson SA, Kayyali TM, DeBold JF, and Miczek KA (2011). Persistent escalation of alcohol drinking in C57BL/6J mice with intermittent access to 20% ethanol. Alcohol Clin Exp Res 35, 1938–1947. 10.1111/j.1530-0277.2011.01545.x. [PubMed: 21631540]

Jensen-Cody SO, Flippo KH, Claflin KE, Yavuz Y, Sapouckey SA, Walters GC, Usachev YM, Atasoy D, Gillum MP, and Potthoff MJ (2020). FGF21 Signals to Glutamatergic Neurons in the Ventromedial Hypothalamus to Suppress Carbohydrate Intake. Cell Metab 32, 273–286 e276. 10.1016/j.cmet.2020.06.008.

Jorgenson E, Thai KK, Hoffmann TJ, Sakoda LC, Kvale MN, Banda Y, Schaefer C, Risch N, Mertens J, Weisner C, and Choquet H (2017). Genetic contributors to variation in alcohol consumption vary by race/ethnicity in a large multi-ethnic genome-wide association study. Mol Psychiatry 22, 1359–1367. 10.1038/mp.2017.101. [PubMed: 28485404]

Koob GF, Roberts AJ, Schulteis G, Parsons LH, Heyser CJ, Hyytia P, Merlo-Pich E, and Weiss F (1998). Neurocircuitry targets in ethanol reward and dependence. Alcohol Clin Exp Res 22, 3–9. [PubMed: 9514280]

Kranzler HR, Zhou H, Kember RL, Vickers Smith R, Justice AC, Damrauer S, Tsao PS, Klarin D, Baras A, Reid J, et al. (2019). Genome-wide association study of alcohol consumption and use disorder in 274,424 individuals from multiple populations. Nat Commun 10, 1499. 10.1038/s41467-019-09480-8. [PubMed: 30940813]

Kurosu H, Choi M, Ogawa Y, Dickson AS, Goetz R, Eliseenkova AV, Mohammadi M, Rosenblatt KP, Kliewer SA, and Kuro OM (2007). Tissue-specific expression of betaKlotho and fibroblast growth factor (FGF) receptor isoforms determines metabolic activity of FGF19 and FGF21. J Biol Chem 282, 26687–26695. 10.1074/jbc.M704165200.

Liu Y, Zhao C, Xiao J, Liu L, Zhang M, Wang C, Wu G, Zheng MH, Xu LM, Chen YP, et al. (2016). Fibroblast growth factor 21 deficiency exacerbates chronic alcohol-induced hepatic steatosis and injury. Sci Rep 6, 31026. 10.1038/srep31026.

Mallard TT, Savage JE, Johnson EC, Huang Y, Edwards AC, Hottenga JJ, Grotzinger AD, Gustavson DE, Jennings MV, Anokhin A, et al. (2021). Item-Level Genome-Wide Association Study of the Alcohol Use Disorders Identification Test in Three Population-Based Cohorts. Am J Psychiatry, appiajp202020091390. 10.1176/appi.ajp.2020.20091390.

Markan KR, Naber MC, Ameka MK, Anderegg MD, Mangelsdorf DJ, Kliewer SA, Mohammadi M, and Potthoff MJ (2014). Circulating FGF21 is liver derived and enhances glucose uptake during refeeding and overfeeding. Diabetes 63, 4057–4063. 10.2337/db14-0595. [PubMed: 25008183]

Millan EZ, Kim HA, and Janak PH (2017). Optogenetic activation of amygdala projections to nucleus accumbens can arrest conditioned and unconditioned alcohol consummatory behavior. Neuroscience 360, 106–117. 10.1016/j.neuroscience.2017.07.044. [PubMed: 28757250]

Namburi P, Beyeler A, Yorozu S, Calhoon GG, Halbert SA, Wichmann R, Holden SS, Mertens KL, Anahtar M, Felix-Ortiz AC, et al. (2015). A circuit mechanism for differentiating positive and negative associations. Nature 520, 675–678. 10.1038/nature14366. [PubMed: 25925480]

Owen BM, Ding X, Morgan DA, Coate KC, Bookout AL, Rahmouni K, Kliewer SA, and Mangelsdorf DJ (2014). FGF21 acts centrally to induce sympathetic nerve activity, energy expenditure, and weight loss. Cell Metab 20, 670–677. 10.1016/j.cmet.2014.07.012. [PubMed: 25130400]

Palmour RM, Mulligan J, Howbert JJ, and Ervin F (1997). Of monkeys and men: vervets and the genetics of human-like behaviors. Am J Hum Genet 61, 481–488. 10.1086/515526. [PubMed: 9326311]

Pomrenze MB, Fetterly TL, Winder DG, and Messing RO (2017). The Corticotropin Releasing Factor Receptor 1 in Alcohol Use Disorder: Still a Valid Drug Target? Alcohol Clin Exp Res 41, 1986–1999. 10.1111/acer.13507. [PubMed: 28940382]

Reed SJ, Lafferty CK, Mendoza JA, Yang AK, Davidson TJ, Grosenick L, Deisseroth K, and Britt JP (2018). Coordinated Reductions in Excitatory Input to the Nucleus Accumbens Underlie Food Consumption. Neuron 99, 1260–1273 e1264. 10.1016/j.neuron.2018.07.051.

Sanchez-Roige S, Fontanillas P, Elson SL, andMe Research T, Gray JC, de Wit H, Davis LK, MacKillop J, and Palmer AA (2019). Genome-wide association study of alcohol use disorder identification test (AUDIT) scores in 20 328 research participants of European ancestry. Addict Biol 24, 121–131. 10.1111/adb.12574. [PubMed: 29058377]

Schumann G, Liu C, O'Reilly P, Gao H, Song P, Xu B, Ruggeri B, Amin N, Jia T, Preis S, et al. (2016). KLB is associated with alcohol drinking, and its gene product beta-Klotho is necessary for FGF21 regulation of alcohol preference. Proc Natl Acad Sci U S A 113, 14372–14377. 10.1073/pnas.1611243113.

Soberg S, Andersen ES, Dalsgaard NB, Jarlhelt I, Hansen NL, Hoffmann N, Vilsboll T, Chenchar A, Jensen M, Grevengoed TJ, et al. (2018). FGF21, a liver hormone that inhibits alcohol intake in mice, increases in human circulation after acute alcohol ingestion and sustained binge drinking at Oktoberfest. Mol Metab 11, 96–103. 10.1016/j.molmet.2018.03.010. [PubMed: 29627377]

Soberg S, Sandholt CH, Jespersen NZ, Toft U, Madsen AL, von Holstein-Rathlou S, Grevengoed TJ, Christensen KB, Bredie WLP, Potthoff MJ, et al. (2017). FGF21 Is a Sugar-Induced Hormone Associated with Sweet Intake and Preference in Humans. Cell Metab 25, 1045–1053 e1046. 10.1016/j.cmet.2017.04.009.

Song P, Zechner C, Hernandez G, Canovas J, Xie Y, Sondhi V, Wagner M, Stadlbauer V, Horvath A, Leber B, et al. (2018). The Hormone FGF21 Stimulates Water Drinking in Response to Ketogenic Diet and Alcohol. Cell Metab 27, 1338–1347 e1334. 10.1016/j.cmet.2018.04.001.

Stefanik MT, and Kalivas PW (2013). Optogenetic dissection of basolateral amygdala projections during cue-induced reinstatement of cocaine seeking. Front Behav Neurosci 7, 213. 10.3389/fnbeh.2013.00213. [PubMed: 24399945]

Stuart T, Butler A, Hoffman P, Hafemeister C, Papalexi E, Mauck WM 3rd, Hao Y, Stoeckius M, Smibert P, and Satija R (2019). Comprehensive Integration of Single-Cell Data. Cell 177, 1888–1902 e1821. 10.1016/j.cell.2019.05.031.

Stuber GD, Britt JP, and Bonci A (2012). Optogenetic modulation of neural circuits that underlie reward seeking. Biol Psychiatry 71, 1061–1067. 10.1016/j.biopsych.2011.11.010. [PubMed: 22196983]

Stuber GD, Sparta DR, Stamatakis AM, van Leeuwen WA, Hardjoprajitno JE, Cho S, Tye KM, Kempadoo KA, Zhang F, Deisseroth K, and Bonci A (2011). Excitatory transmission from the amygdala to nucleus accumbens facilitates reward seeking. Nature 475, 377–380. 10.1038/nature10194. [PubMed: 21716290]

Swift RM, and Aston ER (2015). Pharmacotherapy for alcohol use disorder: current and emerging therapies. Harv Rev Psychiatry 23, 122–133. 10.1097/HRP.0000000000000079. [PubMed: 25747925]

Talukdar S, Owen BM, Song P, Hernandez G, Zhang Y, Zhou Y, Scott WT, Paratala B, Turner T, Smith A, et al. (2016a). FGF21 Regulates Sweet and Alcohol Preference. Cell Metab 23, 344–349. 10.1016/j.cmet.2015.12.008. [PubMed: 26724861]

Talukdar S, Zhou Y, Li D, Rossulek M, Dong J, Somayaji V, Weng Y, Clark R, Lanba A, Owen BM, et al. (2016b). A Long-Acting FGF21 Molecule, PF-05231023, Decreases Body Weight and Improves Lipid Profile in Non-human Primates and Type 2 Diabetic Subjects. Cell Metab 23, 427–440. 10.1016/j.cmet.2016.02.001. [PubMed: 26959184]

Thiele TE (2017). Neuropeptides and Addiction: An Introduction. Int Rev Neurobiol 136, 1–3. 10.1016/bs.irn.2017.07.001. [PubMed: 29056148]

Trudell JR, Messing RO, Mayfield J, and Harris RA (2014). Alcohol dependence: molecular and behavioral evidence. Trends Pharmacol Sci 35, 317–323. 10.1016/j.tips.2014.04.009. [PubMed: 24865944]

von Holstein-Rathlou S, BonDurant LD, Peltekian L, Naber MC, Yin TC, Claflin KE, Urizar AI, Madsen AN, Ratner C, Holst B, et al. (2016). FGF21 Mediates Endocrine Control of Simple Sugar Intake and Sweet Taste Preference by the Liver. Cell Metab 23, 335–343. 10.1016/j.cmet.2015.12.003. [PubMed: 26724858]

Wagner-Skacel J, Horvath A, Grande P, Wenninger J, Matzer F, Fazekas C, Morkl S, Meinitzer A, and Stadlbauer V (2021). Association of fibroblast growth factor 21 with alcohol consumption and alcohol liver cirrhosis. Neuropsychiatr 35, 140–146. 10.1007/s40211-020-00380-8. [PubMed: 33330965]

Wu X, Ge H, Gupte J, Weiszmann J, Shimamoto G, Stevens J, Hawkins N, Lemon B, Shen W, Xu J, et al. (2007). Co-receptor requirements for fibroblast growth factor-19 signaling. J Biol Chem 282, 29069–29072. 10.1074/jbc.C700130200.

Wu YE, Pan L, Zuo Y, Li X, and Hong W (2017). Detecting Activated Cell Populations Using Single-Cell RNA-Seq. Neuron 96, 313–329 e316. 10.1016/j.neuron.2017.09.026.

Ziegenhain C, Vieth B, Parekh S, Reinius B, Guillaumet-Adkins A, Smets M, Leonhardt H, Heyn H, Hellmann I, and Enard W (2017). Comparative Analysis of Single-Cell RNA Sequencing Methods. Mol Cell 65, 631–643 e634. 10.1016/j.molcel.2017.01.023.

Highlights

- An FGF21 analogue suppresses alcohol consumption in non-human primates
- The FGF21 co-receptor KLB is expressed in cells in the basolateral amygdala (BLA)
- FGF21 signals to $KLB^{BLA \rightarrow NAc}$ projecting neurons to suppress alcohol consumption
- FGF21 suppresses sucrose and alcohol consumption through distinct circuits

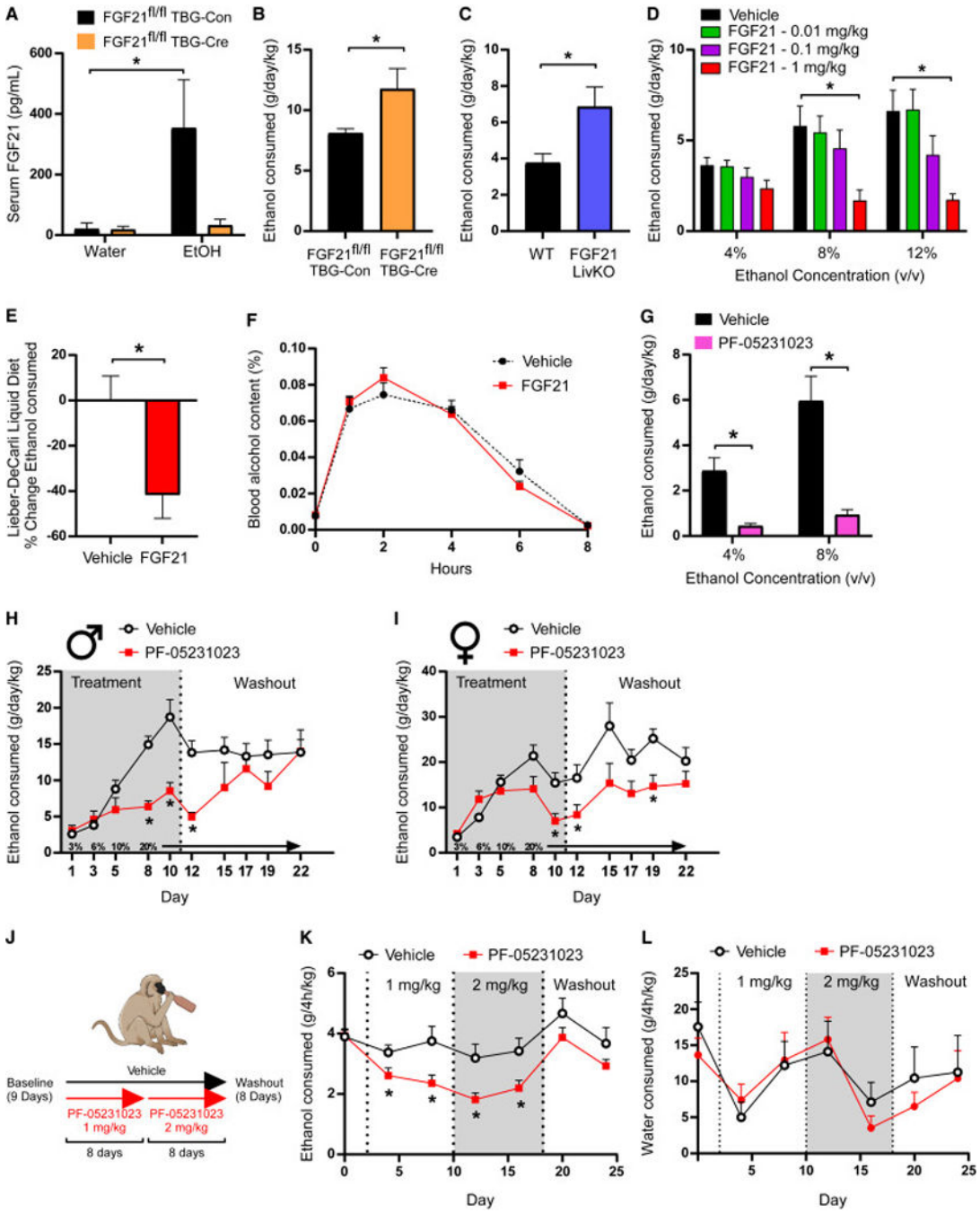

Figure 1. Endogenous and pharmacological FGF21 suppress alcohol consumption in rodents and non-human primates.

(A) Circulating levels of FGF21 in response to water or ethanol gavage (3.5g/kg) in male $FGF21^{fl/fl}$ mice receiving either AAV-TBG-Con or AAV-TBG-Cre (n = 6–8 mice/group, one-way ANOVA, *=P<0.05 relative to mice receiving water gavage).

(B) Ethanol (EtOH) consumption (g/day/kg) in male $FGF21^{fl/fl}$ mice receiving either AAV-TBG-Con or AAV-TBG-Cre allowed ad libitum access to water and EtOH using a 2-bottle choice experimental design (n = 7 and 6/group, respectively, one-tailed unpaired t-test, *=P<0.05).

(C) EtOH consumption (g/day/kg) in male FGF21 liver-specific knockout (FGF21 LivKO) mice and littermate controls allowed ad libitum access to water and EtOH using a 2-bottle choice experimental design (n = 8 and 9/group, respectively, one-tailed unpaired t-test, *=P<0.05).

(D) EtOH consumption (g/day/kg) in wildtype (WT) C57BL/6J male mice treated with the indicated doses of FGF21 (vehicle or mg/kg) via daily intraperitoneal (IP) injection across different EtOH concentrations using a 2-bottle choice experimental design (n = 6 mice/group, 2-way ANOVA w/Holm-Sidak's multiple comparisons test, *=P<0.05 relative to vehicle treated mice for both concentrations).

(E) The percent (%) change in ethanol consumption (12%) in WT C57BL/6J male mice allowed ad libitum access to the Lieber-DeCarli liquid diet receiving daily injections of vehicle or FGF21 (IP, 1mg/kg, n = 12–13 mice/group, two-tailed unpaired t-test, *=P<0.05 relative to vehicle treated mice).

(F) Percent (%) blood alcohol content following EtOH gavage (3.5 g/kg) in WT C57BL/6J male mice treated with vehicle or FGF21 (intraperitoneal (IP), 1 mg/kg) for three days prior to EtOH gavage (n = 5 mice/group).

(G) EtOH consumption (g/day/kg) in WT C57BL/6J male mice treated with a single dose of the FGF21 analogue PF-05231023 (10 mg/kg, IP) or vehicle across different EtOH concentrations using a 2-bottle choice experimental design (n = 11 mice/group, 2-way ANOVA w/Holm-Sidak's multiple comparisons test, *=P<0.05 relative to vehicle treated mice for both concentrations).

(H-I) EtOH consumption (g/day/kg) in WT C57BL/6J male (H) and female (I) mice treated with vehicle or PF-05231023 using the intermittent access paradigm (n = 8 mice/group, 2-way ANOVA w/Two-stage linear step-up procedure of Benjamini, Krieger and Yekutieli, *=P<0.05 when comparing to vehicle treated mice).

(J) A schematic illustration of the experimental design used to assess effect of PF-05231023 on alcohol consumption in alcohol-preferring vervet monkeys in data presented in (K) and (L). Briefly, alcohol-preferring male vervet monkeys (n = 20) were given access to alcohol for 4 h a day for 9 days to establish baseline drinking behavior. After establishing a baseline, vervets were divided into either a placebo (n = 8) or treatment arm (n = 12). Those in the treatment arm received PF-05231023 at an initial dose of 1 mg/kg for 8 days, which was then increased to 2 mg/kg for an additional 8 days. A washout period in which no drug was administered was then performed over 8 days.

(K-L) EtOH consumption (K) and water intake (L) in the indicated treatment groups (2-way ANOVA w/Two-stage linear step-up procedure of Benjamini, Krieger and Yekutieli, *=P<0.05 when comparing to placebo treated animals).

Data are presented as mean ± S.E.M.

See also Figure S1 and Table S1.

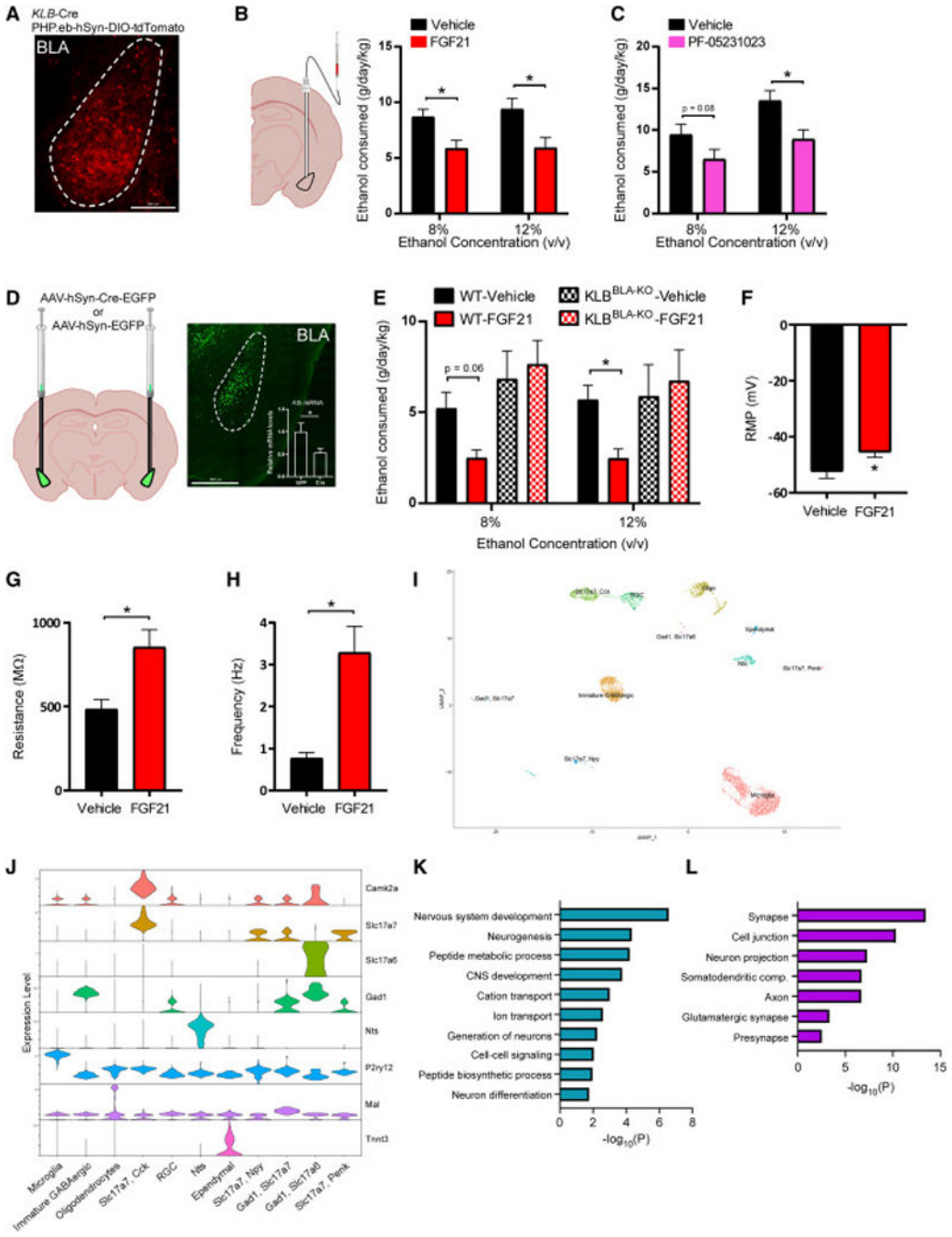

Figure 2. FGF21 signals to KLB expressing neurons in the basolateral amygdala to suppress alcohol consumption.

(A) A representative fluorescent image of tdTomato expressing cells in the basolateral amygdala (BLA) in brain slices generated from KLB-Cre mice 4 weeks following infection with PHP.eB-DIO-tdTomato. Scale bar = 200 μm.

(B) Ethanol (EtOH) consumption (g/day/kg) in WT C57BL6/J mice treated with unilateral delivery of vehicle or FGF21 to the BLA via cannula (0.01 mg/kg) across different EtOH concentrations using a two-bottle choice experimental design (n = 9 and 11 mice/group, respectively).

(C) EtOH consumption (g/day/kg) in WT C57BL6/J mice treated with unilateral delivery of vehicle or PF-05231023 to the BLA via cannula (0.01 mg/kg) across different EtOH concentrations using a two-bottle choice experimental design (n = 8 mice/group for both groups).

(D) Schematic representation of the strategy used to delete KLB in the BLA of $KLB^{fl/fl}$ mice through stereotactic delivery of AAV-hSyn-Cre-EGFP or AAV-hSyn-EGFP (as a control) to the BLA of $KLB^{fl/fl}$ mice. Representative fluorescent image of viral targeting of AAV-hSyn-Cre- EGFP to the BLA of $KLB^{fl/fl}$ mice. In the inset, relative *Klb* mRNA expression in the amygdala of $KLB^{fl/fl}$ mice 4 weeks following delivery of either AAV-hSyn-EGFP or AAV-hSyn-Cre-EGFP is measured (n = 4 and 5 mice/group, respectively, one-tailed unpaired t-test, *=$P<0.05$). Scale bar = 500 μm.

(E) EtOH consumption (g/day/kg) in $KLB^{fl/fl}$ mice 4 weeks following injection of AAV-hSyn-EGFP (WT) or AAV-hSyn-Cre-EGFP ($BLA^{KLB\text{-}KO}$) into the BLA, treated daily with either vehicle or FGF21 (intraperitoneal (IP), 1 mg/kg) across different EtOH concentrations using a two-bottle experimental design (n = 6–9 mice/group).

(F-H) Electrophysiological analysis of (F) resting membrane potential (RMP, mV), (G) membrane resistance (MΩ), and (H) action potential frequency (Hz) in tdTomato expressing neurons in KLB-Cre mice four weeks following retro-orbital delivery of PHP.eB-DIO-tdTomato before (aCSF) and after FGF21 application to acute brain slices (n = 16–30 neurons from at least 3 mice for each analysis, two-tailed paired t-test, *=$P<0.05$ relative to aCSF).

(I) Single cell RNA sequencing of tdTomato expressing cells isolated from the BLA of KLB-Cre; Ai14-tdTomato mice and performed UMAP clustering to identify distinct cell types (RGC = radial glia cell, Nts = Neurotensin).

(J) A violin plot representation of the expression of genes which encode the indicated cell-type markers across clusters in $tdTomato^{+}$ cells isolated from the BLA of KLB-Cre;Ai14-tdTomato mice (RGC = radial glia cell, Nts = Neurotensin).

(K-L) Gene ontology analysis of gene networks associated with (K) biological processes and (L) subcellular compartments significantly upregulated (*P* values on x-axis) in KLB^{+}/$Slc17a7^{+}$ cells isolated from mice treated with FGF21 (1 mg/kg) for 3 days relative to mice treated with vehicle. Data are presented as mean ± S.E.M. 2-way ANOVA w/Holm-Sidak's multiple comparisons test was used for statistical analyses unless stated otherwise, *=$P<0.05$ relative to vehicle treated mice. See also Figure S2 and Table S2.

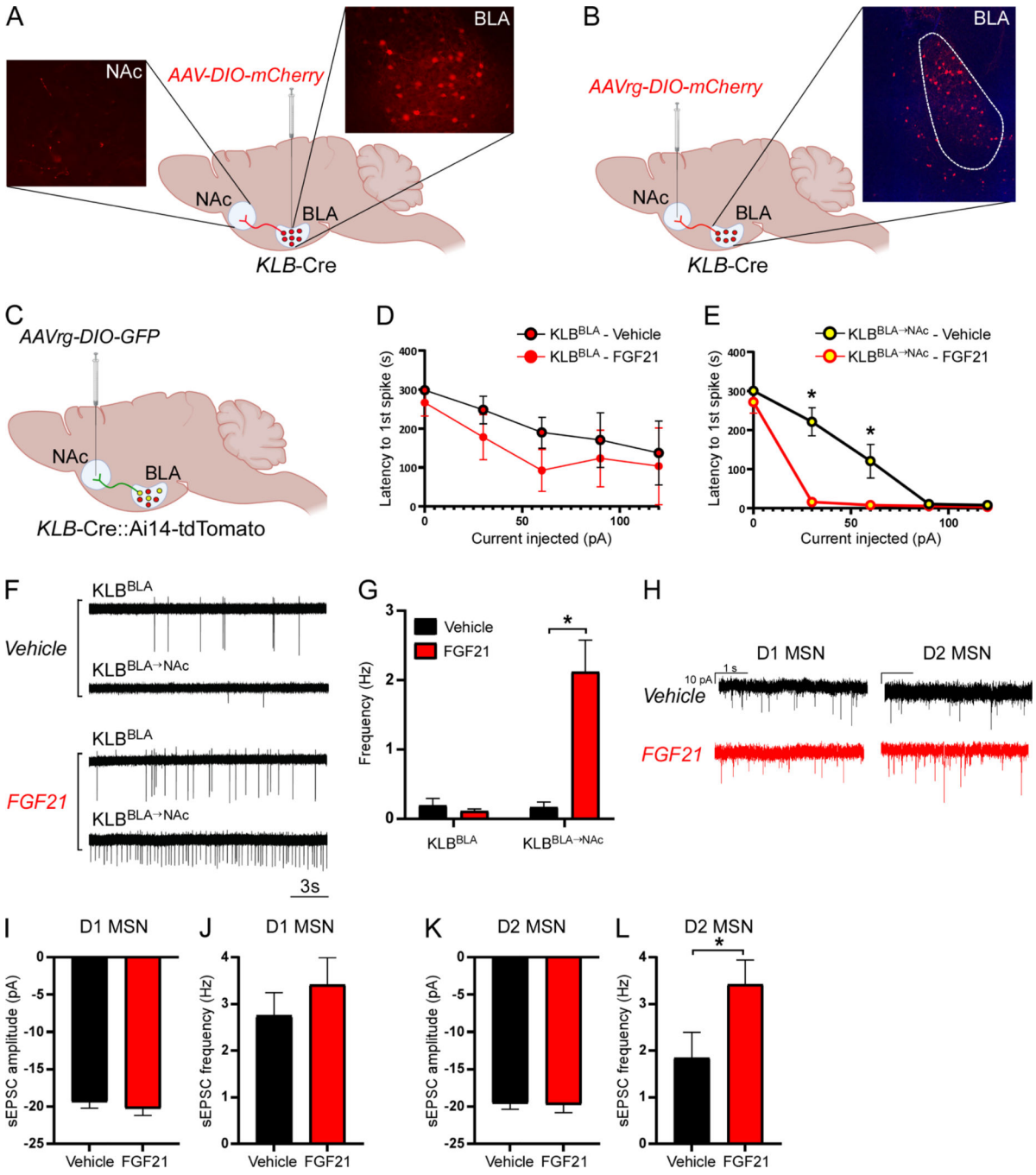

Figure 3. FGF21 preferentially influences excitability of KLB$^{BLA\rightarrow NAc}$ projection neurons and D2 MSNs in the NAc.

(A) A schematic diagram illustrating how stereotactic delivery of AAV-DIO-mCherry to the basolateral amygdala (BLA) of KLB-Cre mice was used to identify downstream projection targets of KLB-expressing (KLB^{+}) neurons in the BLA.

(B) A schematic diagram illustrating how stereotactic delivery of AAVrg-DIO-mCherry to the nucleus accumbens (NAc) was used to confirm that KLB^{+} neurons in the BLA project to the NAc.

(C) A schematic diagram illustrating the strategy used to distinguish between KLB^{+} neurons in the BLA which project to the NAc ($KLB^{BLA\rightarrow NAc}$) and those that do not project to the NAc (KLB^{BLA}). (D-E) Electrophysiological analysis of latency to the first action potential spike correlated with current injection in (D) KLB^{BLA} and (E) $KLB^{BLA\rightarrow NAc}$ neurons in acute brain slices from mice treated with FGF21 (intraperitoneal (IP), 1 mg/kg) or vehicle for 3 days prior to recording (n = 7–12 neurons/group from at least 3 mice/group, 2-way ANOVA w/Holm-Sidak's multiple comparisons test, *=$P<0.05$).

(F) Representative traces of loose seal action current spikes for the data quantified in (G).

(G) Firing frequency (Hz) in acute brain slices from mice treated with FGF21 (IP, 1 mg/kg) or vehicle for 3 days prior to recording (n = 25–52 neurons/group from at least 3 mice/group, 2-way ANOVA w/Sidak's multiple comparisons test, *=$P<0.05$).

(H) Representative traces of spontaneous miniature excitatory post-synaptic currents (sEPSCs) in D1- and putative D2-expressing medium spiny neurons (MSNs) in the NAc core in acute brain slices from mice treated with FGF21 (IP, 1 mg/kg) or vehicle for 3 days prior to recording.

(I-J) sEPSC amplitude and frequency in D1-MSNs in the lateral NAc core in acute brain slices from vehicle and FGF21 treated mice (n = 12–14 neurons/group from at least 3 mice/group).

(K-L) sEPSC amplitude and frequency in putative D2-MSNs in the lateral NAc core in acute brain slices from vehicle and FGF21 treated mice (n = 12–14 neurons/group from at least 3 mice/group, two-tailed unpaired t-test, *=$P<0.05$).

Data are presented as mean ± S.E.M.

See also Figure S3.

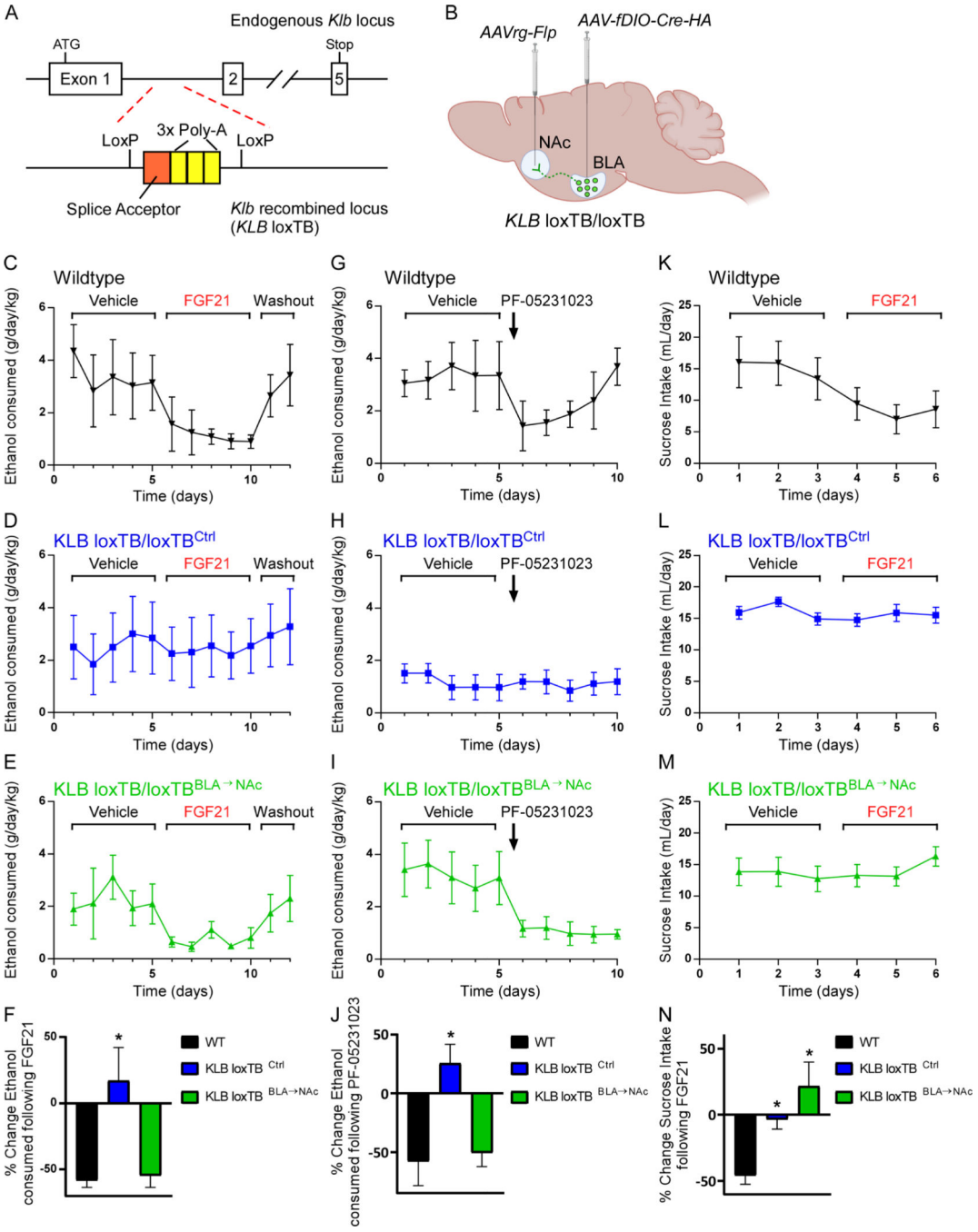

Figure 4. KLB expression in BLA→NAc projection neurons is necessary and sufficient for suppression of alcohol consumption by FGF21 and PF-05231023.

(A) Schematic illustrating placement of a transcriptional blocking sequence (splice acceptor (orange) followed by 3x poly A tail sequence (yellow)) in the intronic region between the 1st and 2nd exon of *Klb* flanked by loxP sites to generate KLB loxTB mice.

(B) Schematic illustrating the dual recombinase strategy used to return endogenous KLB expression specifically to BLA→NAc projecting neurons using an AAVrg-Flp expressing virus injected into the NAc and an AAV virus expressing a Flp-dependent HA-tagged version of Cre (AAV-fDIO-Cre-HA) injected into the BLA.

(C-E) Ethanol (EtOH) consumption (g/day/kg) in wildtype mice (black, WT), KLB loxTB control mice (blue, KLB loxTB^{Ctrl}, KLB$^{loxTB/loxTB}$ mice which received AAV-fDIO-Cre-HA in the BLA, but AAVrg-GFP in the NAc instead of AAVrg-Flp), and mice in which endogenous KLB expression was returned to BLA→NAc projecting neurons (green, KLB loxTB$^{BLA→NAc}$; KLB$^{loxTB/loxTB}$ mice which received AAV-fDIO-Cre-HA in the BLA, and AAVrg-Flp in the NAc) during daily vehicle administration followed by daily FGF21 administration (IP, 1 mg/kg) as indicated by the brackets above the plots followed by a washout period.

(F) Percent (%) change in EtOH consumption comparing FGF21 treatment period relative to the vehicle treated period for each group (n = 5 WT mice, 12 KLB loxTB^{Ctrl}, 9 KLB loxTB$^{BLA→NAc}$, one-way ANOVA w/Dunnett's multiple comparison's test, *=P<0.05 relative to WT mice).

(G-I) EtOH consumption in WT, KLB loxTB^{Ctrl} mice, and KLB loxTB$^{BLA→NAc}$ during daily vehicle administration followed by a single injection of PF-05231023 (IP, 10 mg/kg) as indicated by the brackets and arrow, respectively, above the plots.

(J) Quantification of the percent (%) change in EtOH consumption comparing 1 day following PF-05231023 treatment relative to the vehicle treated period for each group (n = 5 WT mice, 12 KLB loxTB^{Ctrl}, 9 KLB loxTB$^{BLA→NAc}$, one-way ANOVA w/Dunnett's multiple comparison's test, *=P<0.05 relative to WT mice).

(K-M) Sucrose consumption (mL/day) in WT, KLB loxTB^{Ctrl} mice, and KLB loxTB$^{BLA→NAc}$ during daily vehicle administration followed by daily FGF21 administration (IP, 1mg/kg) as indicated by the brackets above the plots.

(N) Quantification of the percent (%) change in sucrose consumption comparing FGF21 treatment period relative to the vehicle treated period for each group (n = 5 WT mice, 12 KLB loxTB^{Ctrl}, 9 KLB loxTB$^{BLA→NAc}$, one-way ANOVA w/Holm-Sidak's multiple comparison's test, *=P<0.05 for KLB loxTB$^{BLA→NAc}$ mice relative to WT mice).

Data are presented as mean ± S.E.M.

See also Figure S3.

KEY RESOURCES TABLE

REAGENT or RESOURCE	SOURCE	IDENTIFIER
Antibodies		
Rabbit α-HA-tag, 1:1000	Cell signaling	3724S
AlexaFluor488-fluorescently-conjugated goat α-rabbit	Life Technologies	A-11070
Bacterial and virus strains		
AAV-hSyn-HI-eGFP-Cre	Addgene	Addgene #: 105540-AAV9
AAV-hSyn-EGFP	Addgene	Addgene #: 50465-AAV9
AAV-hSyn-DIO-mCherry	Addgene	Addgene #: 50459-AAV9 and AAVrg
AAV-hSyn-DIO-EGFP	Addgene	Addgene #: 50457-AAVrg
AAV-EF1a-Flpo	Addgene	Addgene #: 55637-AAVrg
AAV-EF1a-fDIO-Cre	Addgene	Addgene #: 121675-AAV9
AAV-FLEX-tdTomato	Addgene	Addgene #: 28306-PHP.eb
AAV-TBG-PI-Cre	Addgene	Addgene #: 107787-AAV8
AAV-TBG-PI-Null	Addgene	Addgene #: 105536-AAV8
Chemicals, peptides, and recombinant proteins		
Recombinant human FGF21	NovoNordisk	
PF-05231023	Pfizer	
N-Methyl-D-glucamine	Sigma	Cat#:M2004
KCl	Research Products International	Cat#:P41025–500.0
NaCl	Research Products International	Cat#:S23020–500.0
NaH_2PO_4	Research Products International	Cat#:S23185–500.0
$NaHCO_3$	Research Products International	Ca#:S25060–500.0
HEPES	Research Products International	Cat#:H75030–50.0
Glucose	Research Products International	Cat#:G32045–500.0
$MgSO_4$-7H2O	Research Products International	Cat#:M65240–100.0
$CaCl_2$-2H2O	Research Products International	Cat#:C36200–500.0
Sodium Ascorbate	Research Products International	Cat#:S42175–100.0
Thiourea	Sigma	Cat#:T8656
Sodium Pyruvate	Sigma	Cat#:P2256
Pronase	Roche	Cat#: 10165921001
Fetal Bovine Serum	Gibco	Cat#:26140–079
CNQX	Tocris	Cat#:0190
TTX	Tocris	Cat#:1078
D-AP5	Tocris	Cat#:0106
Pertussis Toxin	Tocris	Cat#:3097
Actinomycin D	Sigma	Cat#: A1410
Critical commercial assays		

REAGENT or RESOURCE	SOURCE	IDENTIFIER
Mouse/Rat FGF21 ELISA	Biovendor	Cat#: RD291108200R
BD Rhapsody Whole Transcriptome Analysis Kit	BD Biosciences	Cat#: 633802
Deposited data		
Raw and processed scRNAseq data	Gene Expression Omnibus	GEO: TBD
Experimental models: Organisms/strains		
$FGF21^{fl/fl}$	Markan et al., 2014	
FGF21 LivKO	Markan et al., 2014	
$KLB^{fl/fl}$	Ding et al., 2012	
Ai14-tdTomato	The Jackson Laboratory	007914
KLB-Cre	Jensen-Cody and Flippo et al., 2020	
KLB loxTB mice	This paper	
Oligonucleotides		
Klb: 5' - GATGAAGAATTTCCTAAACCAGGTT-3' , 5' - AACCAAACACGCGGATTTC −3'	von Holstein-Rathlou et al. 2016	
Fgf21: 5'-CCTCTAGGTTTCTTTGCCAACAG-3', 5'-AAGCTGCAGGCCTCAGGAT-3';	von Holstein-Rathlou et al. 2016	
Cre: 5'-TGTTGCCGCGCCATCTG-3', 5'-TTGCTTCAAAAATCCCTTCCA-3'	von Holstein-Rathlou et al. 2016	
U36B4: 5'-CGTCCTCGTTGGAGTGACA-3', 5'-CGGTGCGTCAGGGATTG-3'	von Holstein-Rathlou et al. 2016	
Software and Algorithms		
ImageJ	Schneider et al., 2012	https://imagej.nih.gov/ij/
Seurat	Stuart and Butler et al., 2019	https://satijalab.org/seurat/
BD Rhapsody Analysis pipeline	BD	sbgenomics.com/bdgenomics
Axon pCLAMP 11.3	Molecular Devices	N/A
R	The R Project for Statistical Computing	https://www.r-project.org/
Graphpad Prism 7	Graphpad	http://www.graphpad.com/scientific-software/prism/